# MASS MEASUREMENTS OF BLACK HOLES IN X-RAY TRANSIENTS: IS THERE A MASS GAP?

Laura Kreidberg[1,2], Charles D. Bailyn[1], Will M. Farr[3,4], and Vicky Kalogera[3]

[1] Department of Astronomy, Yale University, New Haven, CT 06520, USA
[2] Department of Astronomy and Astrophysics, University of Chicago, Chicago, IL 60637, USA
[3] Department of Physics and Astronomy and Center for Interdisciplinary Exploration and Research in Astrophysics (CIERA),
Northwestern University, Evanston, IL 60208, USA

## ABSTRACT

We explore possible systematic errors in the mass measurements of stellar mass black holes (BHs). We find that significant errors can arise from the assumption of zero or constant emission from the accretion flow, which is commonly used when determining orbital inclination by modeling ellipsoidal variations. For A0620−00, the system with the best available data, we show that typical data sets and analysis procedures can lead to systematic underestimates of the inclination by $10°$ or more. A careful examination of the available data for the 15 other X-ray transients with low-mass donors suggests that this effect may significantly reduce the BH mass estimates in several other cases, most notably that of GRO J0422+32. Assuming that GRO J0422+32 behaves similarly to A0620−00, the reduction in the mass of GRO J0422+32 fills the mass gap between the low end of the distribution and the maximum theoretical neutron star mass, as has been identified in previous studies. Otherwise, we find that the mass distribution retains other previously identified characteristics, namely a peak around $8\,M_\odot$, a paucity of sources with masses below $5\,M_\odot$, and a sharp drop-off above $10\,M_\odot$.

*Key words:* black hole physics – X-rays: binaries

## 1. INTRODUCTION

Soft X-ray transients (SXTs) provide some of the strongest evidence for the existence of stellar mass black holes (BHs). In these systems, Eddington-limited X-ray outbursts occur over timescales of weeks to months, followed by years to decades of X-ray quiescence (Chen et al. 1997). During quiescence, the optical light from the system is dominated by the companion star. Classic binary star analysis techniques can be used to determine the orbit of the companion star in quiescence, and thus the orbital parameters of the entire system, including precise determinations of the mass of the compact object (Orosz 2003). Many of these mass determinations are greater than the theoretical upper bound of neutron stars ($\approx 3\,M_\odot$), and thus the compact objects are understood to be BHs. These black hole SXTs (BHSXTs) comprise most of the dynamically confirmed stellar mass BHs.

Mass measurements of these systems have been used to explore the distribution of BH masses in X-ray binaries (Bailyn et al. 1998; Özel et al. 2010; Farr et al. 2011). In these studies, published values for the orbital parameters have been used as inputs for a Bayesian analysis of the mass distribution of the compact objects. In all of these analyses, a significant mass gap between the maximum neutron star mass ($3\,M_\odot$) and the low end of the BH mass distribution ($\lesssim 5\,M_\odot$) has been identified. This is a curious result, since one would ordinarily expect that the mass distribution of BHs would be weighted toward the low end, as is the mass distribution of pre-supernova massive stars. Indeed, some theoretical results do not suggest the existence of a mass gap (Fryer & Kalogera 2001), but several alternative theories have been proposed to explain the evolution of massive stars in binary systems and how the resultant supernova explosions might result in such a gap (Brown et al. 2001; Belczynski et al. 2012).

Recently, however, the accuracy of the mass measurements for individual objects has implicitly been questioned. Cantrell et al. (2010, hereafter C10) have reanalyzed all extant data for the prototypical BHSXT A0620−00. Prior to C10, published values for the orbital inclination ranged from $i = 37°$, implying a BH mass of $16\,M_\odot$ (Shahbaz et al. 1994) to $i = 74°$, implying a BH mass of $4\,M_\odot$ (Froning & Robinson 2001) with several intermediate values (Haswell et al. 1993; Gelino et al. 2001). C10 find that this wide range of incompatible results can be reconciled by more careful modeling of the ellipsoidal light curves of the companion star. In particular, C10 cull the data to include only data in the "passive" state (Cantrell et al. 2008), in which the light curves do not exhibit short-term non-ellipsoidal variability. They fit the light curves with a model that includes variable disk light and a hotspot that is allowed to vary in position and brightness. In this way C10 find a consistent value of the orbital inclination, $i = 51°.0 \pm 0°.9$, which implies $m_{BH} = 6.6 \pm 0.25\,M_\odot$.

It is becoming increasingly clear that other BHSXTs have active/passive state changes similar to A0620−00, and may have variable hotspots (e.g., MacDonald et al. 2011). However, the orbital parameter estimates in the literature generally do not take these effects into account. Thus it is possible that, like A0620−00, many of the BHSXTs may have mass estimates that are inaccurate by considerable amounts. In this paper, we examine the systematic errors introduced by the presence of nonstellar flux in the ellipsoidal light curves of BHSXTs, assuming they have time variability characteristics comparable to those of A0620−00. We find that there is likely a bias toward mass estimates that are higher than the true mass of the compact object. We find that the "mass gap" identified in previous work (Bailyn et al. 1998; Özel et al. 2010; Farr et al. 2011) on the mass distribution of BHSXTs may be the result of this systematic effect. Specifically, our correction to the mass of GRO J0422+32 fills in the gap. Further study of this object is required to determine whether our assumption

---
[4] CIERA Postdoctoral Fellow.

that it behaves like A0620−00 is valid. However, previous observations of the source have shown aperiodic variability so pronounced that it obscures the ellipsoidal variations (Reynolds et al. 2007), indicating that the accretion flow makes a substantial contribution to the total flux. As we show in this paper, such nonstellar flux tends to depress inclination measurements made with standard analysis procedures, resulting in inflated mass measurements.

The outline of the paper is as follows. In Section 2, we summarize the primary sources of systematic uncertainty in BH mass measurements. We quantify these uncertainties in Section 3 for A0620−00. In Section 4, we generalize the error estimates obtained for A0620−00 to other systems. Section 5 contains a re-evaluation of the mass estimates for 16 BHSXTs. We use these revised mass estimates to analyze the mass distribution in Section 6, and in Section 7 we conclude.

## 2. SOURCES OF SYSTEMATIC ERROR IN MASS DETERMINATION

The mass $m_{BH}$ of the BH in a BHSXT is determined by three parameters: the mass ratio of the secondary star to the BH, $q \equiv m_*/m_{BH}$, the mass function $f$, and the orbital inclination $i$. Written in terms of these parameters, the BH mass is

$$m_{BH} = \frac{f(1+q)^2}{\sin^3 i}. \tag{1}$$

The error on the mass measurement thus depends on the error in $f$, $q$, and $i$.

The mass function $f$ generally contributes little to the systematic error on BH mass. It is a function of the orbital period $P$ and semiamplitude of the radial velocity curve $K$, $f = PK^3/(2\pi G)$. For most cases, $P$ is measured to sub-percent precision using photometric observations that span many periods. The radial velocity curve amplitude is typically known to within 10%, with precision mainly limited by the resolution of the spectroscopy. Neither measurement is strongly affected by systematic bias. A narrow Gaussian is thus a good approximation of the error on $f$, which introduces a small random error on $m_{BH}$.

The mass ratio $q$ is inferred from the rotational broadening of spectral lines. By inspection of Equation (1), we see that $m_{BH}$ is relatively insensitive to the mass ratio for $q \ll 1$. In 11 of the 16 systems in our sample, $q < 0.15$ (see Table 2). For three systems with larger $q$, the mass ratio is well constrained. The remaining two systems have only an upper limit, $q < 0.5$. Thus in all but these two systems the uncertainty in the measured mass ratio has a small impact on $m_{BH}$.

By far the largest source of systematic error is the orbital inclination. Inclination is typically measured by analyzing ellipsoidal variability in the observed photometric light curve. The origin of this variability is gravitational distortion of the companion star. The star fills its Roche lobe, so as it orbits the BH, the projected surface area and average temperature along the observer's line of sight is not constant. This gives rise to characteristic double peaks in the light curve, known as ellipsoidal variations, whose amplitude depends on the inclination. The largest amplitude occurs for systems edge-on to our line of sight ($i = 90°$), because that geometry maximizes the changes in projected surface area of the star with orbital phase. By contrast, no ellipsoidal variations can be detected for face-on systems ($i = 0°$). One can therefore determine $i$ by modeling ellipsoidal variability in the observed photometric light curve.

The simplest model of ellipsoidal variability is just a simulated Roche lobe-filling star. This model, which we will call

the "star-only" model, is commonly employed in the literature under the assumption that nonstellar sources of light are negligible, particularly in the IR (e.g., Martin et al. 1995; Greene et al. 2001; Gelino & Harrison 2003). However, it has been noted that nonstellar flux can constitute a significant fraction of the total flux from the system, even in the IR (Hynes et al. 2005; Gelino et al. 2010). In the optical, nonstellar sources can contribute more than half the total flux (e.g., Zurita et al. 2002; Orosz et al. 2004; C10). The ratio of nonstellar light to the total flux (hereafter denoted NSL fraction) is thus critical to measuring inclination accurately.

To determine the NSL fraction, one subtracts a template stellar spectrum from the observed spectrum, which reveals the continuum excess due to the nonstellar light (e.g., Marsh et al. 1994). It is not necessarily the case, however, that such a measurement is valid for photometric observations taken at a different date from the spectroscopy. Several sources contribute to the NSL fraction, some of which vary on timescales short compared to the orbital period. These sources include the accretion disk, hotspots on the disk, and potentially a jet. They can distort the shape of the photometric light curve in the following ways.

1. The accretion disk contributes a baseline flux which dilutes the amplitude of the ellipsoidal variations. To first order, increasing the disk flux is degenerate with lowering the inclination.
2. The disk and jet can exhibit aperiodic changes in brightness (flickering) due to the accretion flow (C10). The timescale of this variability is short compared to the orbital period, so flickering can be misinterpreted as photometric error, particularly in folded light curves. However, flickering is not a white noise process, nor is it stationary, so binning and averaging the data will *not* reproduce the underlying ellipsoidal shape.
3. The disk hotspot can also distort the light-curve shape. The hotspot causes a peak in flux once per orbit, which leads to asymmetric light curves when superposed with double-peaked ellipsoidal variability. Moreover, the position of the hotspot is not constant, so it can alternately increase or decrease the amplitude of the ellipsoidal variations for the same source (C10).

Measuring inclination accurately is thus a delicate procedure that requires fitting a light curve with a consistent shape and a known NSL fraction, using a model that includes a disk and a hotspot. Using a less sophisticated model will result in systematically biased inclination measurements. Moreover, because the light-curve shape changes over time, different observing runs will yield different inclination measurements, even if the same model is used to fit the light curve.

## 3. QUANTIFICATION OF SYSTEMATIC ERROR FOR A0620−00

We now characterize the systematic error in inclination measurements due to the effects discussed in the preceding section. Our goal is to determine how inclination measurements obtained with a given model compare to the true inclination of a BHSXT. Specifically, we want to know the distribution of inclination measurements one would obtain from observing a source at many distinct times, and where the true inclination lies within that distribution. This requires two pieces of information: one, an accurate inclination measurement, and two, a description of the time variability of the source.

Such an analysis is possible for the source A0620−00, one of the best-studied BHSXTs. Archival data spans the past 30 years, including eight observing runs and more than a decade of daily photometric monitoring from the Small and Moderate Aperture Research Telescope System (SMARTS) consortium (Cantrell et al. 2008). C10 use this extensive data set to make an inclination measurement that accounts for the systematic errors discussed in Section 2. They restrict the sample of light curves to those in the passive state (when aperiodic variability is minimal). They also require that each individual light curve maintain the same shape over its entire duration. These restrictions limit the sample to 12 light curves. An additional four light curves are removed from the sample due to uncertainty in NSL fraction and magnitude calibration. They fit the eight light curves that remain with a 11 parameter model that includes an accretion disk with variable temperature, size, and flaring angle and a hotspot with variable temperature, size, and position. During the fitting procedure, they constrain the disk to contribute the spectroscopically determined NSL fraction. The best-fit inclinations to all eight light curves are statistically self-consistent, giving a weighted average of $i = 51°0 \pm 0°9$. We assume this value is unbiased by systematic error.

Given an accurate inclination measurement for A0620−00, we now determine how inclination estimates vary with time. First we select all subsets of existing data that resemble plausible observing runs. We fit each of these light curves with a star-only model to obtain a sample of inclination estimates. We chose a star-only model both because it is commonly used and because it introduces a straightforward systematic error.

### 3.1. Distribution of Inclination Measurements from Archival A0620−00 Data

For our analysis, we use data collected by C10. We select all subsets of this data that could be obtained on a typical observing run, i.e., many observations in a short period of time. Specifically, we require each subset to contain at least 20 data points over seven days, with gaps in phase no larger than 0.1. We also specify that subsets do not overlap, ensuring that each point is only counted once. We restrict the sample to light curves of comparable quality to previously published BHSXT light curves by binning the data in 30 phase bins and removing all light curves with average bin deviation greater than 0.03 mag. These selection criteria are less stringent than those of C10 because we seek a sample that reflects the typical quality of all previously analyzed light curves, whereas C10 were careful to select only those light curves that minimize systematic error in inclination measurements. Our final sample consists of 57 light curves taken with four different filters: V, I, H, and W (a wide bandpass centered at 4700 Å).

We fit each light curve with a star-only model to obtain a distribution of inclination estimates. To fit the data, we use the Eclipsing Lightcurve Code (ELC) of Orosz & Hauschildt (2000). Our model star has a mean temperature of 4600 K and a gravity darkening exponent of 0.10, consistent with a K5 spectral type and a convective envelope (Lucy 1967; Gray 1992). Limb darkening is computed directly from the model atmosphere. For each light curve in our data set, we obtain an inclination estimate $\hat{\imath}$ from the model that gives the lowest $\chi^2_{\rm red}$. The distribution of $\hat{\imath}$ for all the light curves is shown in Figure 1. Note that we distinguish the estimated inclination $\hat{\imath}$ from the true inclination, denoted $i$. We find $\hat{\imath}$ ranges from $33°9$ to $52°4$. Over 90% of the measurements fall *below* the C10 measurement of $\hat{\imath} = 51°$. Such systematic underestimation is
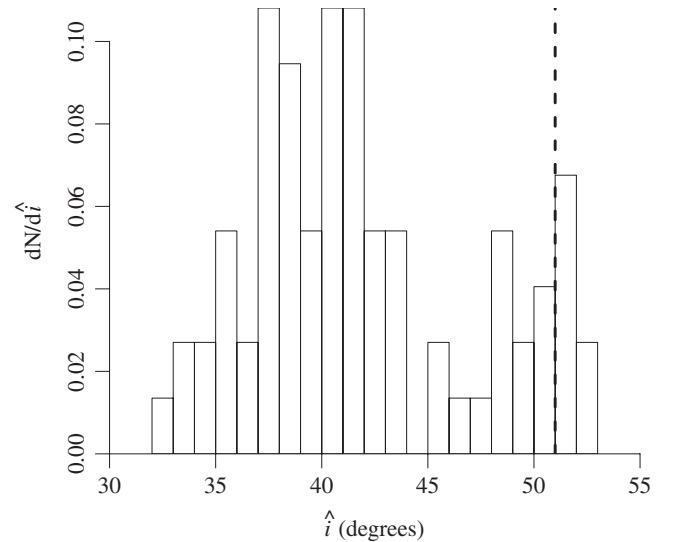


**Figure 1.** Histogram of inclination estimates obtained by fitting a star-only model to extant A0620−00 light curves. Note that 90% of the probability mass lies below the C10 inclination measurement $\hat{\imath} = 51°$, marked in this plot with a thick dashed line.

expected: nonstellar flux almost always dilutes the amplitude of the ellipsoidal variations, mimicking a lower inclination. The few light curves with $\hat{\imath} > 51°$ may be the result of constructive interference between the hotspot and the ellipsoidal variability. The distribution of $\hat{\imath}$ is bimodal, with one peak near $40°$ and the other near $50°$. We discuss potential mechanisms for this bimodality in the next section.

### 3.2. Distribution of Inclinations from Simulated A0620−00 Light Curves

The bimodality in the distribution of inclinations seen in Figure 1 is an intriguing result because it illustrates the potential impact of nonstellar flux on inclination measurements. To explore how different factors contribute to the shape of the distribution, we introduce a method to simulate A0620−00 light curves.

We build on the work of Cantrell et al. (2008), who analyze the time variability of A0620−00 using long-term photometric monitoring from the SMARTS consortium. They identify two distinct states—labeled "active" and "passive"—that occur when the X-ray source is in its quiescent state. In the passive state there is minimal aperiodic variability, so the light-curve shape is stable from night to night. By contrast, flickering is much more pronounced in the active state: active light curves are brighter, bluer, and more variable, possibly due to increased accretion activity. States persist for several months, but transitions from state to state occur on sub-night timescales. A0620−00 is active roughly 70% of the time (C10). Because active and passive data behave differently, we simulate the two states separately.

#### 3.2.1. Simulation of Passive Data

Although passive-state light curves do not change shape on short timescales, passive states separated by a period of activity *do not* necessarily have the same light-curve shape. The eight light curves fit by C10 were passive, but they had significantly different shapes from each other. The main difference between the model fits were the hotspot parameters, suggesting that shape changes in passive light curves are due to the changing temperature and position of the hotspot. Therefore, to model
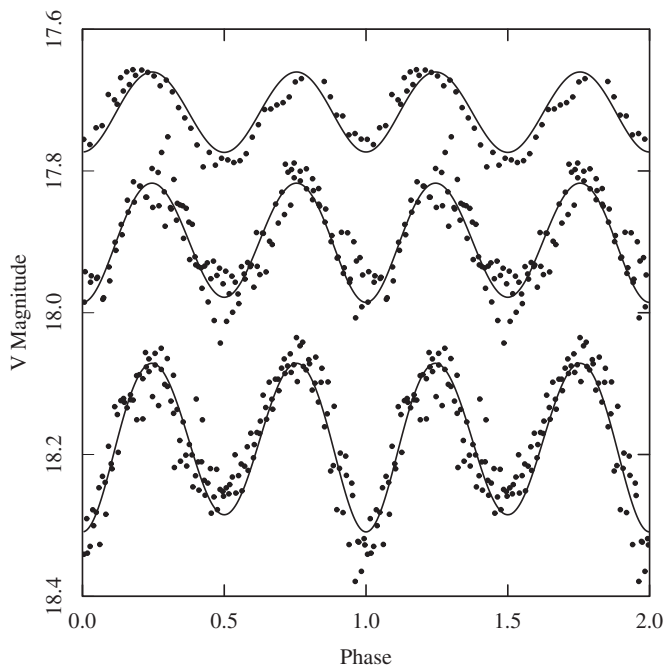
**Figure 2.** Simulated active *V*-band light curves (points). The best-fitting star-only models (lines) have inclinations $i = 30°4$, $37°4$, and $44°9$, with larger ellipsoidal variability corresponding to higher inclination. Each light curve consists of a single night of simulated data.



**Figure 3.** Kernel density estimates for inclination obtained from fitting a star-only model to passive and active light curves (top and bottom panels, respectively). Solid lines correspond to simulated *H*-band data and dashed lines to simulated *V*-band data. All four samples contain 500 light curves. The vertical gray line marks the inclination measurement obtained by C10.

**Table 1**
Hotspot Parameters

| Fit | $s_{spot}$ | $\theta_{spot}$ | $r_{cut}$ | $w_{spot}$ |
|-----|-----------|-----------------|-----------|------------|
| 1 | 7.14 | 341.7 | 0.37 | 33.9 |
| 2 | 2.53 | 200.8 | 0.27 | 31.7 |
| 3 | 1.53 | 19.3 | 0.87 | 90.0 |
| 4 | 2.41 | 199.4 | 0.89 | 89.7 |
| 5 | 5.70 | 190.3 | 0.07 | 70.7 |
| 6 | 4.20 | 102.5 | 0.66 | 85.9 |
| 7 | 6.36 | 72.5 | 0.54 | 39.4 |
| 8 | 5.50 | 37.7 | 0.38 | 20.5 |

**Notes.** This table lists the hotspot parameters for the ELC fits in C10. The ratio of hotspot temperature to disk temperature is $s_{spot}$. The hotspot is centered at azimuthal angle $\theta_{spot}$ and extends from the outer disk to an inner radius $r_{cut}$, given in units of disk radii. The angular radius is given by $w_{spot}$.

passive data, we select hotspot parameters from the range of fits in C10, listed in Table 1 (J. Orosz 2011, private communication). We find no correlation between any of the parameters, so we choose each parameter uniformly between the minimum and maximum value given in Table 1. We use ELC to generate 500 passive *V*- and *H*-band light curves with the specified hotspot parameters. We then add photometric errors drawn from a normal distribution with mean 0 and standard deviation 0.03 mag. A representative sample of simulated light curves is shown in Figure 2. The light curves are fit with a star-only model with parameters described in Section 3.1. All fits had $\chi^2_{red} < 3.0$. We consider the quality of these fits acceptable, since we seek to reproduce typical analysis procedures and $\chi^2_{red}$ has commonly exceeded 2.0 in previously published inclination fits (e.g., Shahbaz et al. 1996; Beekman et al. 1997; van der Hooft et al. 1998). The distribution of best-fit inclinations for each filter is shown in the top panel of Figure 3. These distributions reveal that the A0620−00 hotspot has a greater effect on the
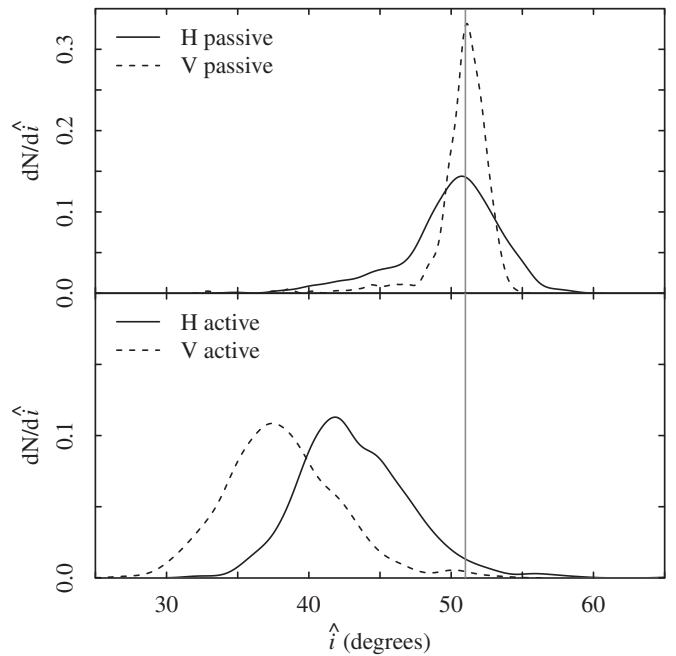
light-curve shape at longer wavelengths. For both filters, the distribution is peaked around $i = 51°$ with some left skew. For an estimator $\hat{\imath}$ obtained by fitting a star-only model to passive data, the true inclination $i$ is given by $i = \hat{\imath}^{+3.3}_{-2.4}$ for *H*-band data and $i = \hat{\imath}^{+1.6}_{-1.1}$ for *V*-band data. The limits denote 68% confidence. These distributions reproduce the second mode in Figure 1, confirming the suggestion that the hotspot can increase or decrease the amplitude of the ellipsoidal variations. The distributions may be artificially narrow: the range of hotspot parameters listed in Table 1 is derived from only eight fits, which probably do not span the entire parameter space. In addition to possible underestimation of the hotspot variability, we neglect all other disk and jet variation. We therefore expect the distribution of $\hat{\imath}$ for passive light curves to be somewhat broader than the results quoted above.

*3.2.2. Simulation of Active Data*

For active-state data, we model the stellar and nonstellar components of the flux separately. We simulate the stellar component with ELC using the same temperature and gravity darkening parameters as in Section 3.1. We set the average stellar magnitude equal to the zero-disk magnitude found in C10.

Next we add a nonstellar component to the stellar light curve. We model the nonstellar flux with a broken power-law power spectral density (PSD). The PSD cannot be determined directly from existing light curves due to severe daily and yearly aliasing. We therefore develop an alternative method to characterize the time variability of the nonstellar flux. We then determine the broken power-law parameters that best reproduce that variability.

We begin by characterizing the time variability of the non-stellar flux. Our data consist of *H*- and *V*-band active-state light curves from the SMARTS consortium, originally published in Cantrell et al. (2008). The *H*-band data set contains 1109 points

over 2227 days and the *V*-band data set contains 634 points over 2755 days. We subtract the ellipsoidal variability from these data using the stellar light curves produced with ELC. The median time between observations is one day; however, there are large seasonal gaps in the data when the object is obscured by the Sun. Even when it is visible, sampling is somewhat sporadic. Due to such uneven sampling, conventional methods to characterize time variability fail. We therefore use a modification of the binned autocorrelation function, denoted $C_\Delta(\tau)$, to describe the time variability.

For the time series $\{(t_1, f_1), \ldots, (t_n, f_n)\}$:

$$C_\Delta(\tau) = \frac{1}{N} \sum_{i=1}^{n} (f_i - \bar{f}(t_i + \tau \pm \Delta))^2, \qquad (2)$$

where $\tau$ is the lag, $\bar{f}(a \pm b)$ is the average of the set $\{f_j\}$ such that $\{t_j\}$ is within the range $a \pm b$, and $N$ is the number of sets where $\{f_j\} \neq \varnothing$.

In other words, $C_\Delta(\tau)$ is the average squared difference for points separated by $\tau \pm \Delta$. If there are no points separated by $\tau \pm \Delta$ (i.e., $N = 0$), $C_\Delta(\tau)$ is undefined. To reduce the number of pairs that are likely to be correlated, we do not include any $(t_i, f_i)$ more than once for a given lag $\tau$. For example, if $\tau = 10.0 \pm 0.05$ and $t = \{0.0, 0.01, 10.0\}$, we remove the pair $\{0.01, 10.0\}$ because $t = 10.0$ has already been included. The error on $C_\Delta$ for a given $\tau$ is the sample standard deviation for the $N$ squared differences. Note that these errors are not Gaussian, because pairs of points separated by $\tau \pm \Delta$ are not statistically independent.

The SMARTS observations provide sufficient coverage to constrain $C_\Delta(\tau)$ for lags on the order of $10^{-1}$–$10^3$ days. The median time difference between observations for both *H*- and *V*-band data is $1.0 \pm 0.05$ days, so we evaluate $C_\Delta(\tau)$ starting at $\tau = 1.0$ and increasing by factors of 2.0 to $\tau = 1024.0$. We choose $\Delta = 0.1$ days. Variability on timescales $< 0.1$ days is small compared to variability for $\tau > 1.0$, so this choice of $\Delta$ does not bias the calculation of $C_\Delta$. For $\tau \leqslant 128.0$ days, this $\Delta$ gives $N > 300$ for both filters. On longer timescales, there are fewer pairs of points from which to choose, so we exclude $\tau$ with $N < 15$. To constrain variability on short timescales, we also compute $C_\Delta(\tau = 0.1$ days) with $\Delta = 0.01$, obtaining $N = 25$ for the *V*-band data and $N = 31$ for H. The results of the calculation of $C_\Delta$ are shown in Figure 4.

We next determine the broken power-law PSD that best matches the $C_\Delta$ statistic for each data set. We assume a PSD $S(f)$ of the form

$$S(f) \propto \begin{cases} \dfrac{1}{f^\alpha} & \text{if } f \leqslant f_b \\[2ex] \dfrac{1}{f_b^{\alpha-\beta} f^\beta} & \text{if } f > f_b, \end{cases} \qquad (3)$$

where $f$ is frequency, $f_b$ is the break frequency, $\alpha$ is the slope at frequencies less than $f_b$, and $\beta$ is slope at frequencies greater than $f_b$.

To find the power-law parameters that best reproduce the observed nonstellar light curve, we implement a grid-based $\chi^2$ minimization routine. We loop over $\alpha$, $\beta$, and $f_b$ and simulate a light curve from each set of parameters following the method of Timmer & Koenig (1995). We normalize the light curve so that it has the same 25% and 75% quartiles as the observed nonstellar light curve. This normalization ensures that outlying data points do not bias the amplitude of the simulated light curve.
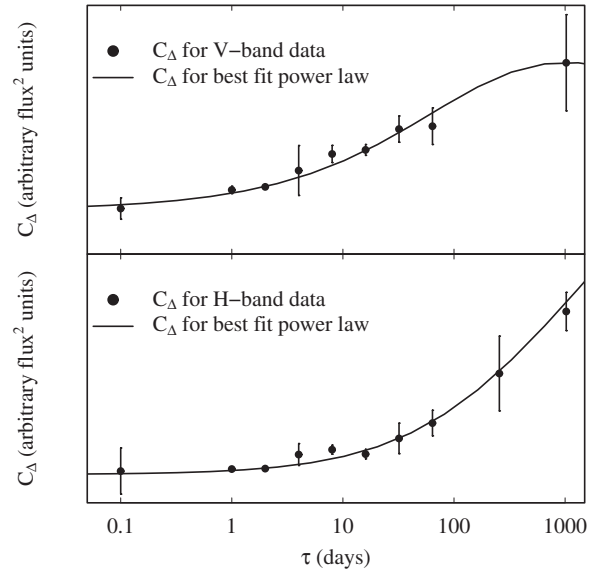


**Figure 4.** Statistic $C_\Delta$ for *V*- and *H*-band SMARTS data (points in the top and bottom panel, respectively) and data generated from the best-fit power law (lines). The value of $C_\Delta$ represents the average squared difference in flux between data points separated by time $\tau \pm \Delta$. The error bars represent the standard deviation of $C_\Delta$ for the $N$ points associated with each $\tau$. The choice of $\tau$ for lags > 256.0 is not identical for the two data sets because they are sampled slightly differently and we require $N > 15$ for each $\tau$. The best-fit power law has parameters $(\alpha, \beta, f_b) = (-0.8, -1.5, 1.2 \times 10^{-8}$ Hz) for *V*-band data and $(-0.8, -1.6, 5.0 \times 10^{-9}$ Hz) for *H*-band data.

We then compute $C_\Delta(\tau)$ for the simulated data and calculate its goodness of fit to $C_\Delta$ for the observed data. We find the power-law parameters that give the minimum $\chi^2$ are $(\alpha, \beta, f_b) = (-0.8^{+0.1}_{-0.0}, -1.5^{+0.7}_{-0.2}, 1.2^{+0.1}_{-0.7} \times 10^{-8}$ Hz) for *V*-band data, with $\chi^2_{\rm red} = 1.7$, and $(-0.8^{+0.7}_{-0.7}, -1.6^{+0.3}_{-0.4}, 5.0^{+8.0}_{-0.0} \times 10^{-9}$ Hz) for *H*-band data, with $\chi^2_{\rm red} = 2.7$. The results for the observed and best-fit simulated light curves are shown in Figure 4. We obtain the uncertainties by holding two parameters fixed and determining the range of the third parameter over which $\chi^2$ increases by a factor of two. These ranges do not represent confidence intervals, nor do we expect $\chi^2_{\rm red} = 1$ for either data set, because the errors on $C_\Delta(\tau)$ are not Gaussian. Nevertheless, varying the parameters within the quoted ranges does not significantly change the distribution of $\hat{\imath}$ obtained from fitting the inclination of the simulated light curves.

To obtain mock active-state data, we simulate fifteen 2500 day long light curves in *V* and *H* using the best-fit power-law parameters. The light curves are sampled at 10 minute intervals. We normalize each light curve such that the 25% and 75% flux quartiles match the observed SMARTS data. We limit the length of the light curves to 2500 days because $C_\Delta(\tau)$ is poorly constrained for $\tau \gtrsim 1000$. In addition, the normalization should be determined using light curves of comparable length. After normalizing the nonstellar light curves, we add back the stellar component of the flux.

In order to select sample data from the 2500 day long simulated light curves, we recreate plausible observing runs in the following way: first, we remove data points during "daylight" hours, assuming 8 hr of viable observing time per 24 hr period. We simulate bad weather by removing 4 hr segments of data with probability 20%. Samples of the light curves are then selected with mock observing runs separated by 30 day intervals. Each run has equal probability of being one, two, or three consecutive days long. We exclude the run from the final sample if it has gaps

5

in phase greater than 0.1. We also bin each run in 30 phase bins and restrict the sample to those runs with average bin standard deviation less than 0.03 mag and none greater than 0.1 mag, as we did for subsets of real data. We select 500 of the remaining light curves for each filter such that the samples are the same size. Several representative light curves are shown in Figure 2. We fit each of the light curves in the sample with the star-only model described in Section 3.1. The resulting estimates of inclination, again denoted $\hat{\imath}$, are shown in the bottom panel of Figure 3. The distributions are approximately normal. We fit a Gaussian to each distribution and find $\hat{\imath} \sim N(38\overset{\circ}{.}2, 4\overset{\circ}{.}0)$ for the $V$-band fits and $\hat{\imath} \sim N(43\overset{\circ}{.}2, 3\overset{\circ}{.}9)$ for the $H$ band, where the notation $N(\mu, \sigma)$ indicates a normal distribution with mean $\mu$ and standard deviation $\sigma$. The relation between true inclination $i$ and the estimator $\hat{\imath}$ is then given by $i \sim N(\hat{\imath} + 12\overset{\circ}{.}8, 4\overset{\circ}{.}0)$ for $V$ and $i \sim N(\hat{\imath} + 7\overset{\circ}{.}8, 3\overset{\circ}{.}9)$ for $H$.

### 3.3. Lessons from A0620−00

Using simulated data, we find that fitting a star-only model to passive-state light curves results in unbiased inclination estimates, approximately normally distributed around the true inclination. The scatter can be explained by a hotspot with changing position and temperature. On the other hand, fitting active data introduces a bias toward artificially low inclination estimates. The typical underestimation is around 8° for IR light curves and 13° for optical light curves. The source of the bias is a significant NSL fraction that increases with shorter wavelength.

These results reproduce the bimodality in inclination estimates obtained from past observations (shown in Figure 1). Whether the source is active or passive is unknown for many of these observations. This is because the C10 procedure for determining optical state uses $V-I$ color, which is unavailable for about half the sample light curves. However, the simulated data reproduces the main characteristics of the distribution shown in Figure 1: the first mode near $\hat{\imath} \sim 40°$ is comparable to the fits to simulated active data, and the second mode around $\hat{\imath} \sim 50°$ is consistent with the simulated passive data fits. In addition, the relative weight of the two modes (roughly 2/3 of the probability mass centered on the first mode) matches the C10 observation that A0620−00 is active around 70% of the time.

## 4. GENERALIZATION OF SYSTEMATIC EFFECTS TO OTHER SYSTEMS

We will now use the description of systematic effects for A0620−00 as a framework to estimate the systematic error on inclination for other sources. We treat passive and active data separately.

For passive A0620−00 data, we found that inclination estimates $\hat{\imath}$ obtained with a star-only model are related to the true inclination $i$ by $i = \hat{\imath}^{+\sigma_1}_{-\sigma_2}$. We assume a similar relation is valid for other systems, because true stellar ellipsoidal variability is dominant in passive light curves. Thus, we expect inclination measurements made using passive data to be unbiased (centered on the true inclination) for all systems. We choose $\sigma_1 = \sigma_2 = 3\overset{\circ}{.}0$. The $\sigma$ values we obtained for A0620−00 are not symmetric and are somewhat smaller; however, as discussed in Section 3.2.1, they are most likely underestimates, so $\sigma = 3\overset{\circ}{.}0$ is a conservative approximation of the error.

For active A0620−00 data, we found

$$i \sim N(\hat{\imath} + \xi, \sigma). \qquad (4)$$

To generalize this result to other systems, we scale the values of $\xi$ and $\sigma$ based on the system's orbital parameters. We find that
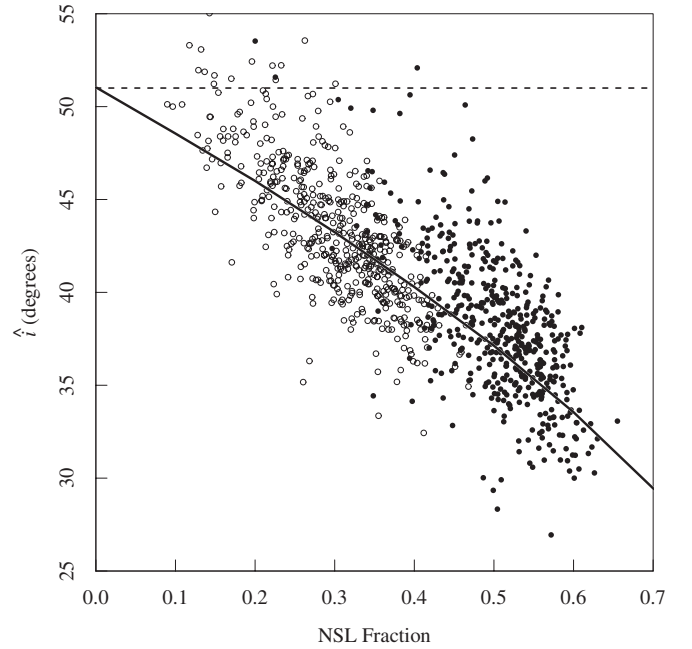


**Figure 5.** Inclination estimates from a star-only model as a function of phase-averaged NSL fraction for simulated active $H$- and $V$-band light curves (open and closed circles). The line gives the inclinations fit to stellar light curves with a constant NSL fraction added. The active light curves have $\hat{\imath}$ within $\pm 2\overset{\circ}{.}7$ of the black curve at 68% confidence. The dashed line marks the inclination measurement of C10, $i = 51\overset{\circ}{.}0$.

$\xi$ can be computed from the NSL fraction, which we denote $\phi$. We discuss this approximation in Section 4.1 and describe a method to estimate the NSL fraction in Section 4.2. We chose $\sigma$ to scale linearly with $\xi$.

### 4.1. Dependence of Inclination Measurements on the NSL Fraction

We expect that the bias in inclination measurements for active data is determined primarily by the NSL fraction, and that flickering and hotspots are secondary effects. To demonstrate this, we simulate a set of light curves with two components: a star and a constant offset flux representing the NSL fraction. We choose $i = 51°$ for the stellar light curve and NSL fractions ranging from 0.0 to 0.9. We fit these diluted light curves with a star-only model to obtain $\hat{\imath}$ as a function of the NSL fraction, $\phi$. A third-order polynomial fit to the results is

$$i - \hat{\imath} = 0.2 + 28.6\phi - 15.3\phi^2 + 27.0\phi^3, \qquad (5)$$

where we take $i = 51°$. We plot this fit in Figure 5 and overplot the points $(\phi, \hat{\imath})$ for each of the simulated A0620−00 active light curves. These points fit the curve closely: the simulated active data have $\hat{\imath}$ within $\pm 2\overset{\circ}{.}7$ of the value obtained from adding a constant NSL fraction (limits denote 68% confidence). We therefore conclude that the NSL fraction is indeed the dominant factor determining the bias $\xi = i - \hat{\imath}$, with some scatter introduced by the disk hotspot and flickering.

### 4.2. Estimating the NSL Fraction Using Orbital Parameters

Given that the NSL fraction determines the bias $\xi$ to first order, we would like to estimate the typical NSL fraction for sources other than A0620−00. Qualitatively, we expect a lower NSL fraction for systems with relatively hotter stars and a higher NSL fraction for systems with relatively larger accretion disks.

To quantify these relationships, we focus on three observable parameters.

1. *Spectral type of the secondary star.* The hotter the star, the greater its total flux contribution and the lower the NSL fraction.
2. *Mass ratio.* The mass ratio determines the relative size of the Roche lobes in the system. Assuming the fraction of the Roche lobe occupied by the disk is constant over all systems, a system with higher $q$ has a relatively larger disk and correspondingly higher $\phi$.
3. *Inclination.* As $i$ increases, the projected area of the disk decreases, thus lowering $\phi$.

To scale the NSL fraction based on the system parameters listed above, we use the Stefan–Boltzmann law. For an optically thick source, the flux scales with the area of the emitting region and the temperature to the fourth power. For convenience, we work with the ratio of stellar to nonstellar flux, which we denote $\rho$. This parameter is related to the NSL fraction by $\rho = 1/\phi - 1$. We expect $\rho$ to scale as

$$\rho \propto \left(\frac{T_{\text{star}}}{T_{\text{disk}}}\right)^4 \left(\frac{R_{\text{star}}}{R_{\text{disk}}}\right)^2 \sec i \qquad (6)$$

$$\propto \left(\frac{T_{\text{star}}}{T_{\text{disk}}}\right)^4 \left(q^{0.45}\right)^2 \sec i, \qquad (7)$$

where $T$ and $R$ denote temperature and effective radius, with subscripts denoting the star and disk. Equation (7) replaces the ratio of radii with $q$ using an approximation from Frank et al. (2002). The $\sec i$ factor accounts for the orientation of the accretion disk, assuming it lies entirely in the orbital plane. We approximate that the star is spherical, so its flux is independent of inclination.

We can use the expression in Equation (7) to estimate the NSL fraction of any source, provided we know the constant of proportionality. To solve for the constant, we use the known parameters for A0620−00. We use the estimates of $q$, $i$, and $T_{\text{star}}$ from C10. We estimate $\rho$ from the simulated active A0620−00 data, obtaining $\rho = 1.0 \pm 0.25$ in the optical and $2.3 \pm 0.6$ in the IR. The remaining unknown is $T_{\text{disk}}$, which we choose to absorb into the constant of proportionality. By neglecting the $T_{\text{disk}}$ dependence, we effectively assume that all sources have the same disk temperature as A0620−00. This approximation is reasonable because the internal dynamics of the disk determine its temperature, not the properties of the gas as it passes through the inner Lagrange point. In addition, this assumption is substantiated by empirical evidence from three cases: the nonstellar light is redder than the B star in SAX J1819.3−2525 (MacDonald et al. 2011), bluer than the K star in A0620−00 (C10), and approximately constant across the optical spectrum for the F star in GRO J1655−40 (A. G. Cantrell 2011, private communication). Under this assumption, we can solve for the proportionality constant in (7) and thus infer $\rho \sec i$ for any system with known $q$ and $T_{\text{star}}$.

We can use our estimate of $\rho \sec i$ to infer the bias $\xi$ in a star-only inclination estimate, $\hat{\imath}$. First, we generate a set of stellar light curves and add a constant flux offset to each such that the ratio of stellar-to-nonstellar flux equals $\rho \sec i$. We vary $i$ from $0°$ to $90°$ in $1°$ intervals. Second, we fit each light curve with a star-only model. We then find the light curve whose inclination estimate is closest to $\hat{\imath}$. Because we know $i$ for this light curve, we can obtain the bias from $\xi = i - \hat{\imath}$ and the NSL
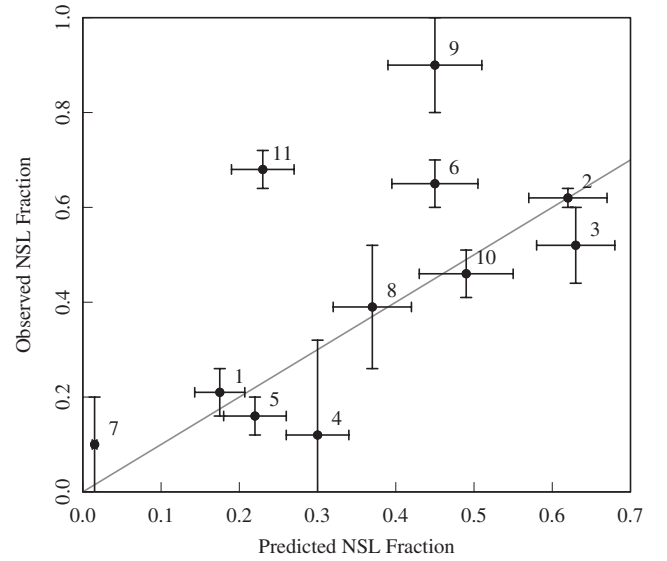


**Figure 6.** Observed vs. predicted optical NSL fractions (points). The gray line is a visual aid representing perfect agreement between the observations and predictions. The numbers indicate the reference for the observation: (1) Orosz et al. 1998; (2) Webb et al. 2000; (3) Casares et al. 1995; (4) Shahbaz et al. 1999; (5) Casares et al. 1993; (6) Filippenko et al. 1999; (7) MacDonald et al. 2011; (8) Orosz et al. 2002; (9) Orosz et al. 2004; (10) Orosz et al. 1996; (11) Wagner et al. 2001. The vertical error bars indicate either $1\sigma$ error or an allowed range. The horizontal error bars reflect the uncertainty due to the variation in the NSL fraction of A0620−00, on which the predictions are based. The excess in the observed NSL fraction for (9) may because the source (GRO J1650−500) was not in full quiescence during the observation. The lack of agreement for source (11) (XTE J1118+480) may be due to this system's high inclination; for large $i$, our assumption that the accretion disk lies entirely in the orbital plane may be invalid.

fraction according to Equation (5). To evaluate the accuracy of this procedure, we compute the NSL fraction from $\rho \sec i$ for all sources with star-only inclination estimates. We compare these values to spectroscopically determined NSL fractions in Figure 6. There is good agreement between our predictions and the observed values, with 7 of 11 predictions within $1\sigma$ from the observed value.

The spread in the NSL fraction of A0620−00 introduces a small amount of scatter in our estimate of $\xi$, generally $< 2°$. This error is unrealistically narrow because it does not include any uncertainty due to other components of the light curve, such as flickering. To estimate the $\sigma$ in Equation (4), we choose the linear relation $\sigma = 3.0 + 0.115\xi$. This scaling reduces to the expression for passive data in the case $\xi = 0°0$ and ensures that $\sigma = 3°9$ for $\xi = 7°8$ (i.e., the values we find for simulated active $H$-band light curves).

### 4.3. Additional Constraints on Inclination

There are two additional constraints on inclination we can obtain. First, we set an upper limit based on the absence of eclipses of the star by the disk. The visibility of eclipses depends on the size of the accretion disk and the mass ratio, $q$. We assume a conservative disk radius of $0.5R_2$ and use ELC to determine the eclipse limit as a function of $q$. Systems with lower $q$ eclipse at higher inclinations, so we use low-end estimates of $q$ to establish secure upper limits on $i$ for the all BHSXTs with measured mass ratios. Specifically, we use the minimum value for mass ratios described by a uniform distribution and the value two standard deviations below the mean for mass ratios with a

**Table 2**
Orbital Parameters for 16 Black Hole Binaries

| X-Ray Name | Optical Counterpart | Spectral Type | $f(M_\odot)$ | $q$ | $i$ (deg) | $i_{min}$ (deg) | $i_{max}$ (deg) | References |
|---|---|---|---|---|---|---|---|---|
| 4U 1543−47 | IL Lup | A2 V | $N(0.25, 0.01)$ | $U(0.25, 0.31)$ | $I(24.0, 36.0)$ | 19.8 | 73.4 | 1, 2 |
| A0620−00 | V616 Mon | K5 V | $N(3.1, 0.04)$ | $N(0.060, 0.004)$ | $N(51.0, 0.9)$ | 36.5 | 79.8 | 3, 4 |
| GRO J0422+32 | V518 Per | M2 +2/−1 V | $N(1.19, 0.02)$ | $N(0.116, 0.08)$ | $N(63.7, 5.2)$ | 0.0 | 90.0 | 7, 8 |
| GRO J1655−40 | V1033 Sco | F6 III | $N(2.73, 0.09)$ | $N(0.38, 0.05)$ | $N(69.0, 3.0)$ | 0.0 | 90.0 | 5, 6 |
| GRS 1009−45 | MM Vel | G5−K7 V | $N(3.17, 0.12)$ | $N(0.137, 0.015)$ | $N(62.0, 5.1)$ | 42.3 | 76.9 | 9, 10, 11 |
| GRS 1124−683 | GU Mus | K3−K4 V | $N(3.01, 0.15)$ | $N(0.128, 0.04)$ | $I(54.0, 65.0)$ | 33.2 | 80.1 | 12, 13 |
| GRS 1915+105 | V1487 Aql | K0-7 III | $N(9.5, 3.0)$ | $N(0.058, 0.033)$ | $N(70.0, 2.0)$ | 0.0 | 90.0 | 14, 15 |
| GS 1354−64 | BW Cir | G0-5 III | $N(5.73, 0.29)$ | $N(0.12, 0.04)$ | $I(27.2, 80.8)$ | 27.2 | 80.8 | 16, 17 |
| GS 2000+25 | QZ Vul | K3-6 V | $N(5.01, 0.12)$ | $N(0.042, 0.012)$ | $I(55.0, 65.0)$ | 28.3 | 86.7 | 18, 19 |
| GS 2023+338 | V404 Cyg | K0 IV | $N(6.08, 0.06)$ | $N(0.060, 0.005)$ | $N(80.1, 5.1)$ | 35.4 | 80.0 | 20 |
| H1705−250 | V2107 Oph | K5 ± 2 V | $N(4.86, 0.13)$ | $U(0, 0.053)$ | $I(48.0, 90.0)$ | 0.0 | 90.0 | 21, 22 |
| SAX J1819.3−2525 | V4641 Sag | B9 III | $N(2.74, 0.12)$ | $N(0.67, 0.04)$ | $I(80.0, 90.0)$ | 44.8 | 69.6 | 23 |
| XTE J1118+480 | KV UMa | K5 V | $N(6.27, 0.04)$ | $N(0.024, 0.009)$ | $I(68.0, 82.0)$ | 21.8 | 89.4 | 24, 25 |
| XTE J1550−564 | V381 Nor | K3 ± 1 III | $N(7.65, 0.38)$ | $U(0.031, 0.037)$ | $I(57.7, 77.1)$ | 26.5 | 82.0 | 26 |
| XTE J1650−500 | ⋯ | G5−K4 III | $N(2.73, 0.56)$ | $U(0, 0.5)$ | $N(75.2, 5.9)$ | 0.0 | 90.0 | 27 |
| XTE J1859+226 | V406 Vul | K5−7 V | $N(4.5, 0.6)$ | $U(0, 0.5)$ | $N(60.0, 3.0)$ | 0.0 | 90.0 | 28 |

**Notes.** This table gives the mass function, mass ratio, spectral type, and inclination estimate for 16 black hole binaries. The measurements of $f$, $q$, and spectral type are taken from the literature. The lower limits on inclination, $i_{min}$, are obtained assuming the secondary has a normal mass for its spectral type. The upper limits, $i_{max}$, are the highest inclinations that do not cause eclipses. For a detailed explanation of these limits and the inclination estimates, see Section 4.

**Notation.** The notation $N(\mu, \sigma)$ implies a normal distribution with mean $\mu$ and standard deviation $\sigma$. A uniform distribution from $\alpha$ to $\beta$ is indicated by $U(\alpha, \beta)$. An isotropic distribution is denoted $i \sim I(\alpha, \beta)$, implying $\cos i$ is uniform between $\alpha$ and $\beta$.

**References.** (1) Orosz 2003; (2) Orosz et al. 1998; (3) Neilsen et al. 2008; (4) Cantrell et al. 2010; (5) Shahbaz et al. 1999; (6) Greene et al. 2001; (7) Webb et al. 2000; (8) Harlaftis et al. 1999; (9) Filippenko et al. 1999; (10) Shahbaz et al. 1996; (11) della Valle et al. 1998; (12) Orosz et al. 1996; (13) Casares et al. 1997; (14) Greiner et al. 2001; (15) Harlaftis & Greiner 2004; (16) Casares et al. 2009; (17) Casares et al. 2004; (18) Harlaftis et al. 1996; (19) Casares et al. 1995; (20) Casares & Charles 1994; (21) Filippenko et al. 1997; (22) Harlaftis et al. 1997; (23) Orosz et al. 2001; (24) González Hernández et al. 2008; (25) Calvelo et al. 2009; (26) Orosz et al. 2011; (27) Orosz et al. 2004; (28) Corral-Santana et al. 2011.

normal distribution. The upper limits calculated according to this procedure are listed in Table 2.

The second constraint on inclination is a lower limit obtained by assuming the secondary star has a mass equal to or less than that of a main-sequence star of its spectral type. A Roche lobe-filling star is out of thermal equilibrium, so the relationship between mass, radius, and surface temperature may be quite different from that of spherical stars. Thus far, undermassive secondaries have been observed in several sources, including GRO J1655−40 (van der Hooft et al. 1997) and A0620−00 (C10). We therefore interpret the standard mass for a secondary star's spectral type as an upper limit to its true mass. If $q$ is known and $m_*$ is overestimated, $m_{BH}$ is also overestimated. By inspection of Equation (1), we find that overestimating $m_{BH}$ results in an underestimation of $i$ for fixed $q$ and $f$. There is some uncertainty in the spectral type for most of the sources in our sample, so to obtain the most stringent lower limit, we calculate $i$ using the mass of the star with the earliest allowed spectral type, along with the low-end estimates for $q$ and $f$ described in the preceding paragraph. If the low-end estimate for $q$ is less than 0.0, the lower limit on $i$ is also $0°.0$. The lower limits on inclination for all sources are listed in Table 2.

## 5. RE-EVALUATION OF INCLINATION AND MASS ESTIMATES FOR TRANSIENT BLACK HOLE BINARIES

Using the procedure established in the previous section, we examine the inclination measurements for the BHs in our sample. Much of the previous work on BH X-ray binaries has had the goal of establishing a lower limit on the mass of the compact object to demonstrate that it is a BH and not a neutron star. As a result, the conservative lower limits on mass are often secure, but the masses and their errors may not be accurate. There are a number of standard practices that may lead to erroneous measurements, which we briefly outline before discussing individual objects in detail.

One of the most frequent assumptions when fitting inclination is that the nonstellar flux is negligible, particularly in the infrared (Shahbaz et al. 1994, 1996; Beekman et al. 1997; Gelino et al. 2001; Greene et al. 2001; Gelino & Harrison 2003). In many cases, this assumption has been justified by claiming the disk spectrum can be modeled as a power law with negative slope, based on the precedent of Oke (1977). The accretion disk thus contributes less total flux in the IR than in the optical. However, this approach has been called into question by recent measurements of significant IR NSL fractions in some sources (Reynolds et al. 2008; Gelino et al. 2010). In addition, there is evidence that the NSL fraction *increases* with wavelength for some objects (Orosz & Bailyn 1997; Reynolds et al. 2007). Inclinations obtained from fitting a star-only model should therefore be treated with caution.

Another common practice when fitting inclination is to combine light curves from two or more observing runs (namely, Shahbaz et al. 1994; Remillard et al. 1996a; Gelino & Harrison 2003; Ioannou et al. 2004; Orosz et al. 2004; Gelino et al. 2006; Casares et al. 2009; Orosz et al. 2011). However, due to aperiodic flickering and migratory hotspots, it is unlikely that combining and/or binning data reproduces the true underlying light-curve shape. In addition, if the data sets being combined have non-overlapping phase coverage, large changes in the light-curve shape may not be detectable. Binning data that have significant intrinsic aperiodic variability tends to depress the amplitude of

the ellipsoidal variations and thus lead to systematically low inclination measurements.

A third potential source of error is using an NSL fraction determined at a different time from the photometric observations. The nonstellar flux can exhibit significant variability on timescales of months, as we show in Section 3.3 for A0620−00. Similar variability has been observed in many other sources, including XTE J1550−564, SAX J1819.3−2525, GRO J0422+32, GS 1354−64, and XTE J1859+226 (Reynolds et al. 2007; Casares et al. 2009; Corral-Santana et al. 2011; MacDonald et al. 2011; Orosz et al. 2011). Given these changes in brightness, it is useful to determine the NSL fraction simultaneously with photometry to obtain an accurate inclination measurement.

In the following section, we examine the data available for each of the 16 BHSXTs in our sample. In particular, we attempt to determine whether the source was observed in an active or passive state. As discussed in Section 3, signatures of the active state include aperiodic variability that is large compared to the quoted photometric errors, high reduced $\chi^2$ values ($\chi^2_{\rm red} > 3$), and significant trends in brightness. The key signatures of passive data are a consistent light-curve shape over the duration of the observations and $\chi^2_{\rm red} < 3$. Using our assessment of the optical state, we determine an appropriate value and error on the inclination, as described in Section 4. In some cases, this results in values of $i$ and hence of the BH mass that are quite different from those in the literature. More extensive observations will be required to check and refine these estimates.

### 5.1. 4U 1543−47

4U 1543−47 is one of the few sources with near simultaneous photometry and spectroscopy. Orosz et al. (1998) analyze $B$-, $V$-, and $I$-band photometry from 1998 June 28 to July 4 and spectroscopy from 1998 July 1 to July 4. The authors determine the NSL fraction in $B$, $V$, $R$, and $I$ from the observed spectrum and use the measurements as constraints when fitting models of ellipsoidal variability to the light curve. Due to the relative brightness of the A-star secondary, we expect the NSL fraction to be small. A larger source of error is the mass ratio, which the authors include as a free parameter in the model. They find $24° < i < 36°$ at the $3\sigma$ level, but note the possibility of additional systematic effects. We therefore use this range as the boundary of a uniform distribution. A more precise measurement, $i \sim N(20°.7, 1°.5)$, was reported in conference proceedings by Orosz et al. (2002). We do not use this measurement because there is no published record of the light curve. However, we note that using this smaller inclination would increase the most likely BH mass by more than a factor of two.

### 5.2. A0620−00

We adopt an inclination measurement of $51° \pm 0°.9$ for A0620−00, based on the analysis of C10. See Section 3 for a discussion.

### 5.3. GRO J1655−40

GRO J1655−40 is a well-studied source, with very regular quiescent light curves (Orosz & Bailyn 1997; Greene et al. 2001; Beer & Podsiadlowski 2002). The consistency in light-curve shape exemplifies the connection between the stellar temperature and the NSL fraction that was discussed in Section 3.3: GRO J1655−50 has a bright F star secondary, so we expect that

it has relatively small NSL fraction, and consequently, a stable light-curve shape. Detailed studies of optical/IR emission and orbital parameters of GRO J1655−40 in full quiescence have been published by Orosz & Bailyn (1997), Greene et al. (2001), and Beer & Podsiadlowski (2002). The Orosz & Bailyn (1997) study gives a tight constraint on $i$ because their modeling requires a partial eclipse of the secondary to account for the depth of the minimum at phase 0.5. By contrast, the Greene et al. (2001) analysis uses a more sophisticated model for limb darkening that allows for a deep primary minimum without eclipses. The Greene et al. (2001) analysis use optical and IR light curves collected between 1999 July 7 and October 30. Over the course of observations, the light curves remained stable within the range of photometric error, a few hundredths of a magnitude. The light curves are also consistent with those reported from several years before by Orosz & Bailyn (1997). Thus these light curves appear to be passive. The data are fit with a star-only model, giving a best-fit inclination $i = 70°.2$ with $\chi^2_{\rm red} = 1.6$. Beer & Podsiadlowski (2002) obtain a similar result by reanalyzing the Orosz & Bailyn (1997) data. They use a model that includes an accretion disk and distance constraints obtained from the kinematics of the radio jet, finding a best-fit inclination of $i = 69°.0$ with $\chi^2_{\rm red} = 1.6$. Recent unpublished measurements of the NSL fraction (A. G. Cantrell 2011, private communication) suggest that the distance to the source obtained by Beer & Podsiadlowski (2002) is more accurate than that of Greene et al. (2001). We therefore adopt the Beer & Podsiadlowski (2002) measurement, which is compatible with the Greene et al. (2001) result, and assume the source was passive during the observations, thus taking $i \sim N(69°.0, 3°.0)$.

### 5.4. GRO J0422+32

GRO J0422+32 has an unusually late-type secondary (Filippenko et al. 1995), and thus we expect the disk contribution to be especially strong. The inclination has been frequently discussed since it was first measured by Orosz & Bailyn (1995). That work finds $i > 45°$ based on $I$-band photometry from 1994 October 27 to October 28. The light curve exhibits noticeable shape changes between the two nights and a difference in mean $I$ magnitude of 0.05. This type of variability is typical of the active state. A lower limit on $i$ is obtained by fitting a star-only model to ellipsoidal variability with amplitude 0.15 mag, an approximate amplitude determined by considering each night in the observed light curve separately. This measurement is consistent with the work of Gelino & Harrison (2003), who find $i = 45° \pm 2°$ from fitting a star-only model to $J$, $H$, and $K'$ light curves. There is evidence, however, for substantial IR disk contamination: Reynolds et al. (2007) detect no ellipsoidal variability in $H$ and $K$ light curves that have mean magnitudes consistent with the Gelino & Harrison (2003) light curves. These conflicting results suggest that both the Gelino & Harrison (2003) and the Reynolds et al. (2007) light curves are in the active state, so we interpret the Gelino & Harrison (2003) measurement as a lower limit. These results are consistent with the work of Filippenko et al. (1995), who find $i = 48° \pm 3°$, assuming a normal mass M2 V secondary and mass ratio $q = 0.1093 \pm 0.0086$. As discussed in Section 4.3, assuming a normal mass secondary gives a lower limit on inclination.

In contrast to the above measurements, there are several works, which find $i < 45°$: Casares et al. (1995) obtain $i = 30° \pm 6°$ for $q = 0.1$, using $I$-band data and assuming zero disk contribution. However, there are significant gaps in phase coverage near the primary maximum at phase 0.25. Another low

measurement is obtained by Callanan et al. (1996), who find $i < 45°$ for an assumed disk contamination less than 0.2. This NSL fraction is based on what is considered typical for other SXTs, which may not be applicable to this source because of the late-type secondary. Moreover, the light curve they fit consists of 14 nights of data between 1994 September 11 and 1995 January 9 that are combined and binned. Given the substantial aperiodic variability this source exhibits, binning data over multiple nights may flatten the light-curve shape, implying a lower inclination. Similarly, Beekman et al. (1997), who find $10° < i < 26°$ use a binned $R$-band light curve obtained between 1995 January 12 and January 15. The light curve consists of just 55 points, binned in phase bins of width 0.1.

Given the large variability exhibited by GRO J0422+32, binning the light curves is unusually problematic. In addition, those measurements fall well below the lower limit obtained using the spectral type of the secondary. Therefore, we discount measurements obtained by binning optical light curves. We adopt $\hat{\imath} = 45°$, assume the source is active, and adjust the inclination according to Section 4, obtaining an inclination $i \sim N(63°.7, 5°.2)$. We note that the $3\sigma$ lower limit of this distribution is consistent with the lower limit of Filippenko et al. (1995). The peak of the probability distribution for the mass of the BH is 2.1 $M_\odot$, which may call into the question the nature of this compact object.

### 5.5. GRS 1009−45

The only analysis of ellipsoidal variability in GRS 1009−45 was performed by Shahbaz et al. (1996). They obtain $R$-band photometry on 1995 May 8–10 and 1996 February 17–21. The light curve shows evidence of aperiodic variability: the peak brightness fluctuates by around 0.1 mag during the time of observations, clear evidence of a significant nonstellar contribution. Shahbaz et al. (1996) bin the data and fit a star-only model, obtaining a best-fit inclination $i = 44°$ with $\chi^2_{red} = 3.2$. Such a high $\chi^2$ indicates that the light curve is most likely active, as is also suggested by the variability. We therefore adjust the inclination estimate $\hat{\imath} = 44°$ according to Section 4, obtaining $i \sim N(62°.0, 5°.1)$.

This result conflicts with the work of Filippenko et al. (1999), who determine inclination assuming the secondary is not undermassive. They find $i = 78°$ for a K7–K8 star with mass $m_* \approx 0.6 M_\odot$. According to the reasoning in Section 4.3, this inclination should be a *lower* limit. However, there is some ambiguity about the spectral type. della Valle et al. (1998) suggest the spectral type may be as early G5 V. Following the procedure outlined in Section 4, we find that a G5 V star implies a lower limit of $\hat{\imath} = 42°.3$, consistent with our estimate $i \sim N(62°.0, 5°.1)$.

### 5.6. GRS 1124−68

GRS 1124−68 is one of the few sources for which simultaneous spectroscopy and photometry exist. Orosz et al. (1996) analyze spectroscopy obtained 1992 April 3 and photometry between 1992 April 3 and April 15 in $I$ and $W$ (the $W$ filter is a wide bandpass centered at 4700 Å). Ellipsoidal modulation is easily discernible in this data. By contrast, long-term monitoring of the source with SMARTS shows no clear ellipsoidal variability since 2003 (C. Bailyn 2012, private communication). We therefore assume the source was passive during the 1992 observations and active post-2003.

Using the 1992 spectroscopy, Orosz et al. (1996) constrain the $B$- + $V$-band NSL fraction to $0.45 \pm 0.05$. Because the source was passive during this period, the NSL fraction is most likely valid for the 12 days of photometry following the spectroscopic observations. Using NSL fractions in the quoted range, Orosz et al. (1996) fit the 1992 $B + V$ light curve with a star + constant flux offset model. However, the $B + V$ light curve has uneven maxima, a signature of the hotspot in the passive state. Fits to the larger maximum yield inclinations above the eclipse limit, so Orosz et al. (1996) fit the smaller maximum and obtain $54° < i < 65°$.

This measurement is somewhat higher and less precise than that of Gelino et al. (2001). They find $i = 54° \pm 1°.5$ from a star-only fit to $J$ and $K$ light curves obtained 2000 February 20–21. However, there is clear evidence for substantial nonstellar flux in the IR (Gelino et al. 2010), when the source was active. The source may have been passive in 2000 February, but that does not guarantee a negligible NSL fraction.

The Orosz et al. (1996) result is also slightly higher than that of Shahbaz et al. (1994), who find $i = 54^{+20}_{-15}°$ for a folded, binned $H$-band light curve from 1995 February 17 to February 20. However, the best-fit inclination gave $\chi^2_{red} = 5.4$, which the authors suggest is a consequence of incorrect sky subtraction and flat-fielding. We therefore adopt the Orosz et al. (1996) result as the most reliable inclination measurement, $54° < i < 65°$.

### 5.7. GRS 1915+105

GRS 1915+105 is the only X-ray binary for which we can measure inclination without analyzing ellipsoidal variability. Greiner et al. (2001) determine an inclination $i = 70° \pm 2°$ based on the apparent superluminal motion of the jet. They assume the jet is perpendicular to the orbital plane due to a lack of observable precession over several years of observation. GRS 1915+105 has been active since its discovery in 1994 (Mirabel & Rodríguez 1994). Single-hump variability and a superhump period have been detected (Bailyn & Buxton 2011), but no studies of ellipsoidal variability have been possible to date because of substantial disk and jet flux variation.

### 5.8. GS 1354−64

Casares et al. (2009) obtain multiwavelength photometry and spectroscopy between 1995 and 2003. The data are characterized by strong aperiodic variability, and no clear ellipsoidal modulation is discernable. Casares et al. (2009) measure an NSL fraction of 0.67 in 2004 and 0.5 in 2006. The average $R$-band magnitude varies by nearly 1 mag between 2002 and 2004. Because of this strong variability, Casares et al. (2009) cannot determine a lower limit to inclination based on ellipsoidal variations. From the spectral type and eclipse limits, we find $27°.2 < i < 80°.8$ according to the criteria in Section 4.3. We assume an isotropic distribution $i \sim I(27°.2, 80°.8)$, indicating that $\cos i$ is uniform between $\cos 27°.2$ and $\cos 80°.8$.

### 5.9. GS 2000+25

The most extensive study of ellipsoidal variability in GS 2000+25 was performed by Ioannou et al. (2004). They obtain $I$-band data from 1992 August and 1998 September, as well as $R$-band data from 1998 September to October, 1999 June, July, and September, and 2000 July to August. The authors note some changes in light-curve shape between the observing runs: for example, the $R$-band light curve has equal maxima in 2000 August, but unequal maxima in 1998 September. These changes are small, however, and there is relatively little scatter in the folded light curve. We therefore conclude that the source

is passive during the Ioannou et al. (2004) observations. The authors bin the light curve and fit a star-only model, finding $54° < i < 60°$. Fits including a disk and hotspot give lower $\chi^2_{\mathrm{red}}$ values, but do not affect the allowed range of inclinations. Fits to data between phase 0.0 and 0.5, which the authors suggest are less affected by the hotspot, also produce the same result. This lack of sensitivity to changes in the model may well be a consequence of combining and binning data taken over many nights: features such as a hotspot are obscured because the hotspot position changes over time. We suspect that binning the data depresses the Ioannou et al. (2004) inclination measurement: even for passive light curves, binning slightly decreases the amplitude of the ellipsoidal variations. Indeed, the Ioannou et al. (2004) measurement is somewhat lower than that of Callanan et al. (1996), who find $55° < i < 65°$ for a star-only fit to $J$ and $K'$ photometry obtained on 1995 August 11–12, assuming $q < 0.05$. The Callanan et al. (1996) result is most likely passive, because it gave a higher inclination range than the passive Ioannou et al. (2004) light curves. Both the Ioannou et al. (2004) and Callanan et al. (1996) results are consistent with the Beekman et al. (1996) estimate $43° < i < 60°$. For our final estimate, we adopt the Callanan et al. (1996) result because it is less affected by binning than that of Ioannou et al. (2004), given that the observations span only two days. We take $i \sim I(55°0, 65°0)$ as our inclination estimate.

### 5.10. GS 2023+338

Strong aperiodic variability in the light curve of GS 2023+388 has thus far prevented precise inclination measurements. Wagner et al. (1992) obtained $I$-band photometry on 17 nights between 1990 September and 1992 May. During this period, the average $I$ magnitude varied by more than 0.1 mag, so the authors are only able to constrain $50° < i < 80°$. The lower limit is derived based on the observation of double-peaked Balmer lines in the spectrum, and the upper limit is based on the lack of eclipses. Shahbaz et al. (1994) find a similar allowed range, $45° < \hat{i} < 83°$, using $K$ and $K'$ photometry obtained between 1992 August and 1993 December. Their best fit with a star-only model has $\hat{i} = 56.0$ with a $\chi^2_{\mathrm{red}} = 15.2$. They suggest the poorness of the fit may be due to an incorrect color correction between the $K$ and $K'$ data. We therefore regard the limits obtained by Wagner et al. (1992) as more secure.

Sanwal et al. (1996) also fit a star-only model to IR data: they obtain $H$-band photometry on 17 nights between 1993 June and November. Strong aperiodic variability is present in the light curve. The authors note that there is significantly more scatter in the observations of GS 2023+388 than in the light curve of the comparison star. They also note a systematic increase in brightness over one 6 hr period of observation. At the beginning of that night, the data are fainter than the ellipsoidal model, but the source smoothly increases in brightness over 6 hr until it is nearly 0.1 mag brighter than the model light curve. This hour-scale time variability suggests that the source was active during these observations. Such behavior is typical of the active state. On the other hand, Khargharia et al. (2010) find almost no disk contamination in the IR spectrum. However, these data were obtained in 2007, and thus do not speak to the state of the system when the Sanwal et al. (1996) data were taken over a decade earlier. We therefore use the minimum inclination estimate of Sanwal et al. (1996), $\hat{i} > 62°0$, which they obtain using a star-only model with standard limb and gravity darkening. We assume that the source was active at the time. Using the method

described in Section 4, we obtain $i \sim N(80°1, 5°1)$. We note that this is approximately equal to the eclipse limit.

### 5.11. H1705−250

The inclination of H1705−250 was first measured by Martin et al. (1995). They obtain 87 $R$-band images on 1992 May 1–6 and fit a star-only model, finding $48° < i < 51°$. The best fit had $\chi^2_{\mathrm{red}} = 0.87$. The authors only show a folded light curve, so it is difficult to detect aperiodic variability.

Remillard et al. (1996b) obtain a conflicting result using $B + V$ observations from 1992 May, 1993 April, and 1994 July. The light curve exhibits uneven maxima, which suggests the source was active during the observations. However, the authors suggest this may be an artifact of changes in phase coverage between the observations. They find a lower limit on $i$ by fitting a star-only model to the light curve, excluding the higher maximum from the fit. Their fit restricts $i > 60°$.

Given the uncertainty in whether the source was active or passive for both these analyses, we adopt the Martin et al. (1995) $i = 48°$ estimate as a lower limit. We cannot obtain an upper limit due to eclipses for this source because the limits on the mass ratio extend to 0.0. Our final estimate for the inclination is thus $i \sim I(48°0, 90°0)$.

### 5.12. SAX J1819.3−2525

Orosz et al. (2001) analyze the photographic $B$-band light curve obtained by Goranskij (1990). The photometric errors are large (near 0.1 mag), so the binned light curve is imprecise. The best-fit model to the light curve has $i = 70°$ and a partial eclipse of the secondary by a large, faint accretion disk; however, it systematically underestimates the amplitude of the ellipsoidal variability.

MacDonald et al. (2011) have compiled 10 years of data on this source, which they separate into clearly defined passive and active states. Analysis of the passive data shows no nonstellar contribution, a result that is supported in some cases by simultaneous spectroscopy. However, the amplitude of the ellipsoidal variability requires an extreme inclination of $\sim 90°$. The X-ray data are sparse enough that an eclipse geometry cannot be excluded. Therefore, we adopt $i \sim I(80°0, 90°0)$.

### 5.13. XTE J1118+480

There is consensus in the literature that XTE J1118+480 has a high inclination, in the range $68° < i < 81°$. However, there are a number of factors that make an accurate measurement challenging. One is a strong superhump modulation in addition to the ellipsoidal variability (Zurita et al. 2002). Another complicating aspect is the large and variable NSL fraction: Wagner et al. (2001) measure an $R$-band NSL fraction of 0.72 for 2000 November 30 which decreases to 0.64 by 2001 January 4.

Gelino et al. (2006) obtain data in $B, V, R, J, H$, and $K$ that may be passive. Their $R$-band light curve is around 0.8 mag fainter than that of Wagner et al. (2001), and there is no detectable superhump period, both indications of less disk activity. They fit data in all bands simultaneously and constrain the NSL fraction in each band. They find $i = 68° \pm 2°$. However, the authors assume there is zero disk contamination in the $H$ band when fitting the spectral template, an assumption that may be problematic.

Wagner et al. (2001) measure $i = 81° \pm 2°$ with a star+disk model using a *brighter* $R$-band light curve than that of Gelino

et al. ([2006](#)). This is unusual, because light curves with very high levels of disk contamination generally cause lower inclination measurements. However, these data were taken on three separate occasions between 2000 December 14 and 2001 January 9, during which time the measured $R$-band disk fraction varied significantly. Moreover, the light curve consists of 68 exposures that were binned in 25 phase bins. The combination of binning small amounts of data taken weeks apart during a period of intense disk activity may lead to an unrepresentative light-curve shape.

McClintock et al. ([2001](#)) also measure a very high inclination, finding a best fit $i = 80°$ for a disk fraction of 0.66. However, they acknowledge uncertainty in the NSL fraction and set a lower limit $i > 40°$ for zero disk light.

The most extensive study of ellipsoidal variability in XTE J1118+480 is that of Zurita et al. ([2002](#)). They obtain $R$-band photometry on 53 unique nights between 2000 December and 2001 June. They observe a steady decrease in magnitude over this time interval, so they detrend the light curve by subtracting the average nightly flux. This light curve shows evidence of superhump modulation and may be distorted by flickering on sub-orbital timescales. They infer an NSL fraction for the detrended light curve by extrapolating the 2001 April measurement of Wagner et al. ([2001](#)) and assuming the decline in brightness is due to a decrease in disk flux. Using the extrapolated NSL fraction, they find an inclination in the range $71° < i < 82°$.

None of the inclination measurements discussed above are free of significant systematic sources of error; they are, however, reasonably consistent. We adopt the full range of inclination estimates obtained for this object, taking $i \sim I(68°.0, 82°.0)$.

### 5.14. XTE J1550−564

Orosz et al. ([2011](#)) determine the inclination of XTE J1550−564 using photometry and spectroscopy obtained between 2001 and 2008. The photometric observations include optical data from 2001 June and NIR data taken between 2006 and 2008. The measured $V$- and $R$-band NSL fractions are 0.3 and 0.39 using 2001 and 2008 spectroscopy, respectively. There are definite changes in the NIR light-curve shape between 2006–2007 and 2008, so it unlikely that the 2008 NSL fraction measurement is valid for the 2006–2007 observations. It is also unlikely that the 2001 NSL fraction is valid for any of the NIR observations. Orosz et al. ([2011](#)) acknowledge this uncertainty, but fit the data using eight different combinations of light curves and NSL fractions. There are four data subsets: optical data only, optical data and 2006–2007 NIR data, optical data and 2008 NIR data, and all optical and NIR data. Each subset is fit separately for both NSL fraction measurements. The model includes a disk with four free parameters: radius, flaring angle, inner radius temperature, and temperature profile. The lowest $\chi^2_{red}$ is obtained using the optical light curves from 2001 and the 2008 NSL fraction. However, as discussed in Section [3.3](#), using NSL fractions determined at a different time from the observations produces unreliable inclination measurements. Nevertheless, the range of inclination measurements from all eight combinations is reasonably narrow: $57°.7 < i < 77°.1$. Because we do not know which of the combinations is most appropriate, we adopt $i \sim I(57°.7, 77°.1)$ as our estimate of inclination. We followed the same reasoning to obtain an estimate for the mass ratio, assuming $q$ is uniformly distributed between the minimum and maximum values found by Orosz et al. ([2011](#)).

### 5.15. XTE J1650−500

Orosz et al. ([2004](#)) determine the inclination of J1650−500 with $R$-band photometry obtained between 2003 May and August. The authors set a lower limit on inclination of $i > 50°$ by fitting a star-only model. Orosz et al. ([2004](#)) also attempt to constrain the NSL fraction using spectroscopy from 2002 June, tentatively finding disk contamination near 0.8 in the $R$ band. There is no indication, however, that this measurement is applicable to the 2003 photometry. No $\chi^2_{red}$ is given for the star-only fit, but we infer that the source was active for the 2003 observations because there appears to be more scatter in the folded light curve than one expects due to photometric error. We therefore assume the source was active and scale the lower limit $\hat{i} = 50°$ according to Section [4](#), which implies $i \sim N(75°.2, 5°.9)$.

### 5.16. XTE J1859+226

Corral-Santana et al. ([2011](#)) obtain $R$-band photometry on 2008 July 31–August 1 and 2010 July 13–14. They compare this data to the 2002 $R$-band light curve of Zurita et al. ([2002](#)) and find an increase in brightness of ∼0.25 from 2002 to 2008 and ∼1.0 from 2002 to 2010. No clear ellipsoidal modulation is detectable in the 2010 data, but the 2000 and 2008 data show variability with amplitude 0.3–0.4 mag, consistent with the passive state. Corral-Santana et al. ([2011](#)) find that a star-only model with $i = 60°$ reproduces these data. We therefore adopt this value as representative of the passive state, and estimate $i = 60° \pm 3°.0$.

## 6. THE BLACK HOLE MASS DISTRIBUTION

We now analyze the mass distribution of BHs using the orbital parameters and new inclination estimates listed in Table [2](#). Previous analyses of the mass distribution indicate that there is a "mass gap," or dearth of BHs, between the maximum theoretical neutron star mass ($\approx 3\,M_{\odot}$) and the minimum BH mass (Bailyn et al. [1998](#); Özel et al. [2010](#); Farr et al. [2011](#)). The presence of a mass gap has important implications for the physics of BH formation, as discussed by Belczynski et al. ([2012](#)).

Based on our arguments in Section [5](#) that many of these published masses may be overestimates, it is plausible that the mass gap inferred in earlier work is the result of systematic errors in mass measurements. Using the revised system parameters in Table [2](#), we show in Section [6.3](#) that there is no evidence of a mass gap, even when using models of the BH mass distribution that give strong evidence for a gap in previous analyses. We demonstrate in Section [6.3](#) that this conclusion rests on the properties of one system in our sample, GRO J0422+32. However, it is not clear that the inclination correction we have identified by analogy to A0620−00 is entirely appropriate for this system; we discuss this issue in Section 6.3.1. Further observations of the system will be needed to settle this question.

### 6.1. Statistical Methods

To address the impact of systematic error in the mass distribution, we repeat a subset of the Bayesian analysis in Farr et al. ([2011](#)) using the adjusted inclination measurements discussed in Section [5](#). Using the distributions of system parameters from Table [2](#), we can compute the probability distribution for the true mass of each system. Figure [7](#) shows these distributions for all 16 BHSXTs.
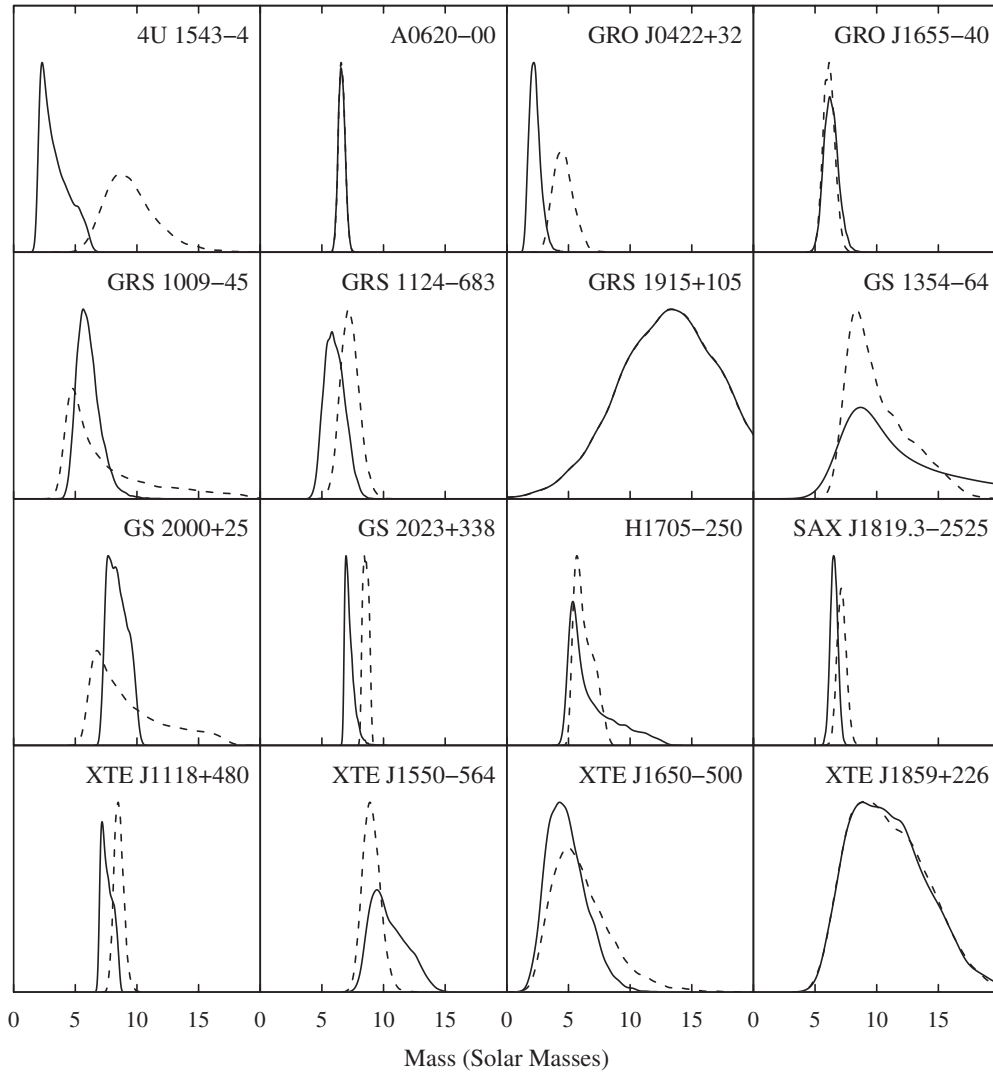
**Figure 7.** Kernel density estimates of the probability distributions for black hole mass implied by the system parameters in Table 2 (solid lines). The distributions implied by the system parameters used in Farr et al. (2011) are also shown (dashed lines). Each panel is normalized so that the probability distributions integrate to 1.

For a set of parameters, $\theta$, governing the underlying BH mass distribution and observational data, $D$, Bayes' rule states

$$P(\theta \mid D) = \frac{P(D \mid \theta)P(\theta)}{P(D)}. \quad (8)$$

Here $P(\theta|D)$, called the *posterior*, is the probability of obtaining particular values for $\theta$ given the observational data, $D$. $P(D \mid \theta)$ called the *likelihood*, is the probability of obtaining the observed data, $D$, when the underlying mass distribution is described by parameters $\theta$. $P(\theta)$, called the *prior*, is the probability distribution one would expect for the parameters before seeing the data. $P(D)$, called the *evidence*, is a normalization constant that ensures that the posterior is a proper probability distribution on parameter space.

Our data $D$ are the set of probability distributions for the underlying masses derived from the observations discussed in Section 5 and displayed in Figure 7. Write $P_i(m_{\rm BH})$ for the distribution of masses in system $i$. We assume that the mass measurements for the 16 systems are independent; then the likelihood is given by

$$P(D \mid \theta) = \prod_i \int P(m_{\rm BH} \mid \theta)P_i(m_{\rm BH})dm_{\rm BH}. \quad (9)$$

It is possible to evaluate the posterior in Equation (8) directly for various values of the parameters, $\theta$. However, this calculation is computationally expensive in multi-dimensional parameter space. As a more efficient alternative, we draw parameter *samples* from the posterior distribution via Markov Chain Monte Carlo methods (Metropolis et al. 1953; Farr et al. 2011). Given a set of samples, $\{\theta_i\}$, one can compute probability distributions for individual parameters by histogram and can approximate posterior-weighted integrals over parameter space by sums

$$\langle f(\theta) \rangle_{p(\theta|D)} = \int d\theta \, f(\theta)p(\theta \mid D) \approx \frac{1}{N} \sum_i f(\theta_i). \quad (10)$$

### 6.2. Model

We focus on the power-law model from Farr et al. (2011, Equation (7)) because it was the most-favored model for the LMXB mass distribution out of the 10 considered in that work.[5]

--------

[5] We have verified that the qualitative behavior of the mass gap described in this section is present for the other models of the LMXB mass distribution considered in Farr et al. (2011).
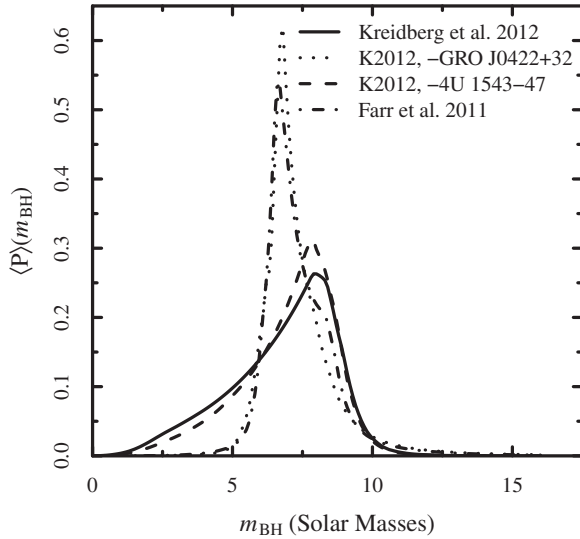
13

**Figure 8.** Marginalized mass distribution, Equation (15), for the power-law mass distribution model (Equation (11)). The solid curve from an analysis using the system parameters in Table 2; the dotted curve from an analysis with the parameters from Table 2, but *excluding* GRO J0422+32 from the sample; the dashed curve comes from an analysis with system parameters from Table 2, but *excluding* 4U 1543−47 from the sample; and the dot-dashed curve comes from the analysis using the system parameters of Farr et al. (2011). The analysis using parameters from Table 2 shows significant support in the gap region, but this conclusion depends strongly on the updated parameters for GRO J0422+32.
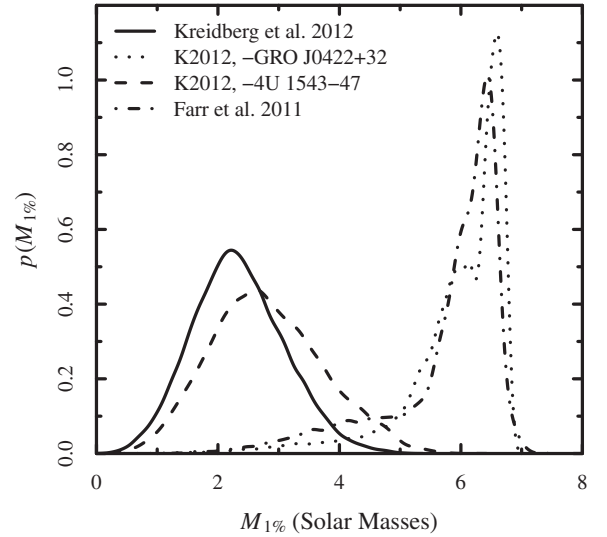


**Figure 9.** Distribution of the 1% mass quantile, $M_{1\%}$, in the power-law model implied by the analysis with system parameters from Table 2 (solid line); parameters from Table 2, but excluding GRO J0422+32 (dotted line); parameters from Table 2, but excluding 4U 1543−47 (dashed line); and parameters from Farr et al. (2011; dot-dashed line). For the complete set of parameters from Table 2, and this set excluding 4U 1543−47, the range of likely minimum black hole masses extends through the gap ($M_{1\%} \lesssim 4\,M_\odot$); when GRO J0422+32 is excluded the minimum black hole mass is equivalent to the analysis from Farr et al. (2011).

The power-law model has

$$P(m_{\rm BH}|\{M_{\min}, M_{\max}, \alpha\}) = \begin{cases} A m_{\rm BH}^\alpha & M_{\min} \leqslant m_{\rm BH} \leqslant M_{\max}, \\ 0 & \text{otherwise} \end{cases}, \tag{11}$$

with parameters

$$\theta = \{M_{\min}, M_{\max}, \alpha\}. \tag{12}$$

The normalization constant, $A$, is

$$A = \frac{1+\alpha}{M_{\max}^{1+\alpha} - M_{\min}^{1+\alpha}}. \tag{13}$$

We use uniform priors on $M_{\min}$, $M_{\max} > M_{\min}$, and $\alpha$ within broad ranges that allow for BH masses up to $40\,M_\odot$:

$$P(\theta) = \begin{cases} 2\frac{1}{40^2}\frac{1}{28} & 0 \leqslant M_{\min} \leqslant M_{\max} \leqslant 40, -15 \leqslant \alpha \leqslant 13 \\ 0 & \text{otherwise} \end{cases}. \tag{14}$$

In the analysis of Farr et al. (2011), the power-law model had strong evidence of a mass gap between the theoretical maximum mass of the heaviest neutron stars ($\sim 3\,M_\odot$) and the mass of the lightest BHs, defined as the 1% quantile ($M_{1\%}$) of the mass distribution in Equation (11). Farr et al. (2011) had $M_{1\%} > 4.3\,M_\odot$ with 90% confidence for the power-law model.

### 6.3. The Mass Gap

With the revised system parameters in Table 2, there are two systems whose mass distribution peaks below $4\,M_\odot$: 4U 1543−47 and GRO J0422+32. Thus, it is not surprising that the expected mass distribution under the power-law model, defined by

$$\langle P \rangle(m_{\rm BH}) \equiv \int d\theta\, P(m_{\rm BH}\,|\,\theta) P(\theta\,|\,D) \tag{15}$$

gains support in the mass gap. That is, the existence of two sources whose mass distribution is strongly peaked below $4\,M_\odot$ necessarily requires that the overall mass distribution not be zero in that region. In Figure 8, we show the $\langle P \rangle(m_{\rm BH})$ implied by the Farr et al. (2011) analysis and the $\langle P \rangle(m_{\rm BH})$ implied by the system parameters in Table 2. Interestingly, the extra support in the gap region is due almost completely to the shift in the mass distribution of GRO J0422+32; in Figure 8 we also show $\langle P \rangle(m_{\rm BH})$ with parameters from Table 2, but *excluding* GRO J0422+32 from the sample, and similarly for excluding 4U 1543−47. When 4U 1543−47 is excluded from the analysis, the curve is essentially the same as when the entire set of 16 systems is analyzed, while excluding GRO J0422+32 produces a curve that is very close to that of Farr et al. (2011).

Another way to address the presence of the mass gap is to examine the posterior probability distribution of the 1% mass quantile, $M_{1\%}$. Figure 9 shows this distribution from the Farr et al. (2011) parameter values, the updated parameters in Table 2, and using the updated parameters but excluding 4U 1543−47 or GRO J0422+32. The analysis using the complete set of systems from Table 2 has significant probability for $M_{1\%} \lesssim 3\,M_\odot$; so does the analysis with parameters from Table 2, but excluding 4U 1543−47. On the other hand, the analysis with parameters from Farr et al. (2011) and Table 2, but excluding GRO J0422+32, have $M_{1\%} \gtrsim 4.3\,M_\odot$ with 90% confidence. Thus, the presence or absence of a mass gap depends strongly on the properties of the mass distribution for GRO J0422+32. In addition, if in the future the mass distribution of 4U 1543−47 were constrained to a narrow peak near the low-mass end of its current distribution, this system would also provide strong evidence against a mass gap. Because the continued evidence for or against the mass gap may depend on the constraints on these systems from future observations, we next discuss the current status of observations of these systems in more detail.
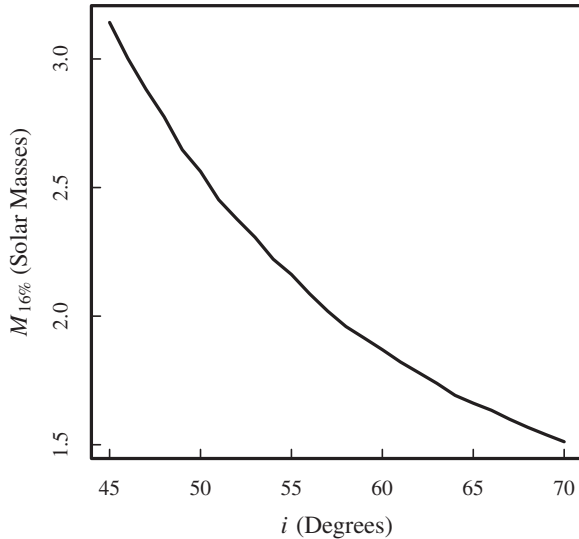
**Figure 10.** Variation in the 16% quantile of J0422+32's mass distribution, $m_{16\%}$, with the assumed peak of the inclination distribution for this object. $m_{16\%}$ is a rough proxy for the peak of the $M_{1\%}$ distribution (see Figure 9). As long as the inclination of J0422+32 is peaks at $i \gtrsim 45°$ we expect to obtain no evidence for a mass gap.

### 6.3.1. GRO J0422+32

The inclination of GRO J0422+32 hinges on whether this source is generally observed in an active state, and whether that active state biases the inclination measurements in a similar way to that of A0620−00. GRO J0422+32 is an unusual system and different in several ways from A0620−00. For example, it does not appear to exhibit a soft state during outburst (Sunyaev et al. 1993). The source also exhibited bright radio emission for nearly a year (Shrader et al. 1994), in contrast to a timescale of months for A0620−00 and other sources (Kuulkers et al. 1999). GRO J0422+32 has also shown noticeable variability in quiescence, with ellipsoidal modulations visible only some of the time (e.g., Gelino & Harrison 2003; Reynolds et al. 2007). It has one of the smallest orbital periods, one of the coolest companion stars, and an extreme mass ratio. Therefore, the ratio of flux from the companion star to that of the disk is expected to be small, and we thus expect that systematic effects due to neglecting the NSL fraction will be pronounced for this system.

If the typical measurements of $i \sim 45°$ for GRO J0422+32 are correct, then the previously identified mass gap still exists. However, if the analogy with A0620−00 is correct, then the inclination must be significantly larger. In this case, the compact object in this system must be roughly between 2 and 3 solar masses, which effectively fills the mass gap (see the relevant panel in Figure 7). In Figure 10, we show how the 16% quantile of J0422+32's mass distribution varies as its inclination distribution's mean varies from the previously accepted value to the value in Table 2, holding the width of the inclination distribution fixed. The 16% quantile approximately tracks the peak of the $M_{1\%}$ distribution shown in Figure 9, so we can see the effect on the mass gap from varying the inclination without repeating the analysis for each value of $i$. We expect to obtain no evidence of a mass gap as long as the inclination distribution of J0422+32 peaks at $i \gtrsim 45°$.

In many ways, GRO J0422+32 is just the kind of system one would expect to be heavily biased by nonstellar light. The secondary star is one of the smallest and coolest of the entire sample. Therefore, changes in the nonstellar flux will

be reflected strongly in the overall flux of the system. And indeed, GRO J0422+32 is quite faint in quiescence ($R \sim 21$) and strongly varying light curves are observed at different times (compare Curry et al. 2003; Gelino & Harrison 2003). Thus, it seems likely that the observed light curves of this source are distorted by nonstellar light in ways that change strongly with time. Whether these distortions conspire to create significant underestimates in the inclination, as in A0620−00, is not yet clear. One route to resolving this issue would be to carry out simultaneous photometry and spectroscopy of GRO J0422+32, so that the division of stellar and nonstellar light can be determined for each individual observation, resulting in an unbiased light curve of stellar light only. However, given the faintness of this source, such observations will be challenging.

### 6.3.2. 4U1543−47

The other source which has a mass probability distribution significantly lower than in previous work is 4U1543−47. This is because we did not accept the Orosz et al. (2002) inclination value, since no published light curve accompanied that report, but rather accepted the earlier, significantly higher estimate of Orosz et al. (1998). That previous higher inclination measurement resulted in a significantly smaller BH mass, but still allowed masses above 4 $M_\odot$, so the source does not greatly affect the possibility of a mass gap. However, if the observations become more precise at the higher inclination value this source might also be an issue for the mass gap, so we discuss it further here.

The difficulties with 4U1543−47 are associated primarily with its low inclination. The $\sin^3 i$ term in Equation (1) means that at low inclination very small changes in $i$ create large changes in the BH mass. Going from the Orosz et al. (2002) result of $i \simeq 20°$ to the previous result centered around $i \simeq 30°$ results in a change in the centroid of the probability distribution of the BH mass of more than a factor of two. At low inclinations, the amplitude of the ellipsoidal modulation is also quite small ($\lesssim 0.1$ magnitudes in this case), so high precision magnitude measurements are required. Given that errors of a few degrees in inclination determinations seem inevitable, it may prove difficult to pin down the inclination of 4U 1543−47 sufficiently tightly to fully resolve the issue.

4U 1543−47 does have some observational advantages, however. It is one of the three sources (with SAX 1819.3−2525 and GRO J1655−40) that have early-type secondaries. These systems all have very regular ellipsoidal variations in the passive state, with very little nonstellar light; this is presumably because the relatively hot secondary stars are particularly bright. Like the other early secondary systems, 4U1543−47 is quite bright in quiescence ($V \sim 15$) so that also makes the system easy to study. There is one technical difficulty in studying 4U1543−47: it is in the wings of an even brighter star, but this can be dealt with through appropriate use of point-spread function fitting techniques. A long-term photometric data set for this source, similar to those for A0620−00 (C10) and SAX1819.3−2525 (MacDonald et al. 2011) has been obtained and is currently being analyzed.

### 6.4. Discussion

A resolution of the specific situation of GRO J0422+32 and 4U1543−47 will be required to determine whether a true mass gap exists in the BHSXT mass distribution. However, even if these two objects do prove to have $M < 4\,M_\odot$, it is still true that the mass distribution rises from the low-mass end. Thus, the

relative paucity of low-mass BHs in these systems still requires an explanation. The peak of the mass distribution appears to be around 8 $M_\odot$, slightly higher than in the previous analysis by Farr et al. (2011). The new analysis also confirms another aspect of the previous analysis, namely, a sharp cutoff above 10 $M_\odot$. This is quite different for the BHSXT BH distribution than for the wind-fed systems with $M_{star} > M_{BH}$ (e.g., Cyg X-1 and M33 X-7), which often contain much more massive BHs. The difference presumably arises due to the dramatically different evolutionary scenarios that create these two kinds of systems (Valsecchi et al. 2010; Wong et al. 2012). It is important to avoid combining these two kinds of systems into a single mass distribution, since there are clearly significant empirical and evolutionary differences between them.

The characteristics of the BHSXT mass distribution should provide guidance and constraints for the physics of massive core collapse. Previous studies have discussed possibilities for observational biases and/or physical mechanisms that can explain the characteristics of the low-mass BH distribution in these systems (Brown et al. 2001; Fryer & Kalogera 2001; Özel et al. 2010). Most recently, Belczynski et al. (2012) have carefully assessed how this low-mass tail and the potential presence of a gap leads to constraints regarding the timescale for the instability growth that eventually drives the stellar explosion, as well as the role of binary evolution in affected the BH masses in low-mass X-ray transients. Our current results, with the mass gap partially filled in, still provide an empirical basis for exploring the physical processes considered in these studies, although the constraints on the explosion timescale will be weaker.

## 7. CONCLUSIONS

We have explored the systematic effects of nonstellar light on the mass estimates of BHs in BHSXTs. We summarize our conclusions as follows.

1. By examining the case of A0620−00, for which the most extensive and carefully analyzed data set exists, we find that observations in the "active" state significantly underestimate the inclination of the system, and consequently overestimate the BH mass. By contrast, observations in the "passive" state appear to be relatively unbiased toward the system inclination.

2. We estimate how large such effects might be in other systems, based on the assumption that the accretion flows are roughly similar in form, while the temperature of the star and the relative size of the star and the accretion disk vary from system to system. The assumption of similar accretion flows appears to be in good agreement with spectroscopic measurements of the NSL fractions.

3. We re-examine the literature on the 16 known BHs in SXTs. The data and analysis of many of these systems have been aimed at establishing a firm minimum for the mass of the compact object, since that is what establishes the identity of the compact object as a BH. When examined from the point of view of determining accurate inclinations, and thus accurate BH masses, we identify a number of problematic issues. These problems stem from the presence of variable nonstellar light, even in the IR. The amount of this extra flux can vary significantly from one observation run to another, and thus it is not safe to use a measurement of stellar light fraction from one time to calibrate photometric observations made at another time. The nonstellar light also appears to vary with orbital phase, so the assumption that it is a flat "dilution" of the ellipsoidal variations is not always true. Significant variability also means that phase binning over long periods of time may result in a light curve that is unrepresentative of the underlying ellipsoidal variations.

4. When we apply a consistent set of criteria to the existing literature on BHSXTs, we find that two objects, GRO J0422+32 and 4U1543−47, may have small BH masses (below 4–5 $M_\odot$, see Figure 7). Specifically, the low mass required for GRO J0422+32 eliminates the mass gap identified in previous work on the BH distribution. But this result depends on the active state of GRO J0422+32 biasing the inclination measurement in the same way as in A0620−00. While this seems plausible, additional observational work will be required to assess whether the active state is indeed biasing the BH mass in this system. We note that if GRO J0422+32 is excluded from the analysis presented here, the results from previous studies, including the mass gap, are reproduced quite closely.

5. However, even if GRO J0422+32 (and possibly 4U1543−47) do fall into the purported mass gap, the basic features of the mass distribution of BHSXTs remain: there are relatively few low-mass ($< 5 M_\odot$) BHs, there is a peak in the distribution around 7–8 $M_\odot$ and a sharp drop-off in numbers beyond 10 $M_\odot$. This distribution is quite different from the "high-mass" BH binary systems, and provides interesting constraints on the supernovae and binary evolution processes that create BHSXTs.

## REFERENCES

Bailyn, C. D., & Buxton, M. 2011, BAAS, 43, 229.05
Bailyn, C. D., Jain, R. K., Coppi, P., & Orosz, J. A. 1998, ApJ, 499, 367
Beekman, G., Shahbaz, T., Naylor, T., & Charles, P. A. 1996, MNRAS, 281, L1
Beekman, G., Shahbaz, T., Naylor, T., et al. 1997, MNRAS, 290, 303
Beer, M. E., & Podsiadlowski, P. 2002, MNRAS, 331, 351
Belczynski, K., Wiktorowicz, G., Fryer, C., Holz, D., & Kalogera, V. 2012, ApJ, in press (arXiv:1110.1635)
Brown, G. E., Heger, A., Langer, N., et al. 2001, New Astron., 6, 457
Callanan, P. J., Garcia, M. R., Filippenko, A. V., McLean, I., & Teplitz, H. 1996, ApJ, 470, L57
Calvelo, D. E., Vrtilek, S. D., Steeghs, D., et al. 2009, MNRAS, 399, 539
Cantrell, A. G., Bailyn, C. D., McClintock, J. E., & Orosz, J. A. 2008, ApJ, 673, L159
Cantrell, A. G., Bailyn, C. D., Orosz, J. A., et al. 2010, ApJ, 710, 1127
Casares, J., & Charles, P. A. 1994, MNRAS, 271, L5
Casares, J., Charles, P. A., Naylor, T., & Pavlenko, E. P. 1993, MNRAS, 265, 834
Casares, J., Martin, E. L., Charles, P. A., Molaro, P., & Rebolo, R. 1997, New Astron., 1, 299
Casares, J., Martin, A. C., Charles, P. A., et al. 1995, MNRAS, 276, L35
Casares, J., Orosz, J. A., Zurita, C., et al. 2009, ApJS, 181, 238
Casares, J., Zurita, C., Shahbaz, T., Charles, P. A., & Fender, R. P. 2004, ApJ, 613, L133
Chen, W., Shrader, C. R., & Livio, M. 1997, ApJ, 491, 312
Corral-Santana, J. M., Casares, J., Shahbaz, T., et al. 2011, MNRAS, 413, L15
Curry, S. M., Bailyn, C., & Buxton, M. 2003, BAAS, 35, 1331

della Valle, M., Masetti, N., & Bianchini, A. 1998, A&A, 329, 606
Farr, W. M., Sravan, N., Cantrell, A., et al. 2011, ApJ, 741, 103
Filippenko, A. V., Leonard, D. C., Matheson, T., et al. 1999, PASP, 111, 969
Filippenko, A. V., Matheson, T., & Ho, L. C. 1995, ApJ, 455, 614
Filippenko, A. V., Matheson, T., Leonard, D. C., Barth, A. J., & van Dyk, S. D. 1997, PASP, 109, 461
Frank, J., King, A., & Raine, D. J. (ed.) 2002, Accretion Power in Astrophysics (3rd ed.; Cambridge: Cambridge Univ. Press), 398
Froning, C. S., & Robinson, E. L. 2001, AJ, 121, 2212
Fryer, C. L., & Kalogera, V. 2001, ApJ, 554, 548
Gelino, D. M., Balman, Ş., Kızıloğlu, Ü., et al. 2006, ApJ, 642, 438
Gelino, D. M., Gelino, C. R., & Harrison, T. E. 2010, ApJ, 718, 1
Gelino, D. M., & Harrison, T. E. 2003, ApJ, 599, 1254
Gelino, D. M., Harrison, T. E., & McNamara, B. J. 2001, AJ, 122, 971
González Hernández, J. I., Rebolo, R., Israelian, G., et al. 2008, ApJ, 679, 732
Goranskij, V. P. 1990, Inf. Bull. Var. Stars, 3464, 1
Gray, D. F. 1992, The Observation and Analysis of Stellar Photospheres (Cambridge: Cambridge Univ. Press)
Greene, J., Bailyn, C. D., & Orosz, J. A. 2001, ApJ, 554, 1290
Greiner, J., Cuby, J. G., & McCaughrean, M. J. 2001, Nature, 414, 522
Harlaftis, E., Collier, S., Horne, K., & Filippenko, A. V. 1999, A&A, 341, 491
Harlaftis, E. T., & Greiner, J. 2004, A&A, 414, L13
Harlaftis, E. T., Horne, K., & Filippenko, A. V. 1996, PASP, 108, 762
Harlaftis, E. T., Steeghs, D., Horne, K., & Filippenko, A. V. 1997, AJ, 114, 1170
Haswell, C. A., Robinson, E. L., Horne, K., Stiening, R. F., & Abbott, T. M. C. 1993, ApJ, 411, 802
Hynes, R. I., Robinson, E. L., & Bitner, M. 2005, ApJ, 630, 405
Ioannou, Z., Robinson, E. L., Welsh, W. F., & Haswell, C. A. 2004, AJ, 127, 481
Khargharia, J., Froning, C. S., & Robinson, E. L. 2010, ApJ, 716, 1105
Kuulkers, E., Fender, R. P., Spencer, R. E., Davis, R. J., & Morison, I. 1999, MNRAS, 306, 919
Lucy, L. B. 1967, Z. Astrophys., 65, 89
MacDonald, R. K. D., Bailyn, C. D., & Cantrell, A. G. 2011, BAAS, 43, 144.20
Marsh, T. R., Robinson, E. L., & Wood, J. H. 1994, MNRAS, 266, 137
Martin, A. C., Casares, J., Charles, P. A., van der Hooft, F., & van Paradijs, J. 1995, MNRAS, 274, L46
McClintock, J. E., Haswell, C. A., Garcia, M. R., et al. 2001, ApJ, 555, 477
Metropolis, N., Rosenbluth, A. W., Rosenbluth, M. N., Teller, A. H., & Teller, E. 1953, J. Chem. Phys., 21, 1087
Mirabel, I. F., & Rodríguez, L. F. 1994, Nature, 371, 46
Neilsen, J., Steeghs, D., & Vrtilek, S. D. 2008, MNRAS, 384, 849

Oke, J. B. 1977, ApJ, 217, 181
Orosz, J. A. 2003, in IAU Symp., 212, A Massive Star Odyssey: From Main Sequence to Supernova, ed. K. van der Hucht, A. Herrero, & C. Esteban (Cambridge: Cambridge Univ. Press), 365
Orosz, J. A., & Bailyn, C. D. 1995, ApJ, 446, L59
Orosz, J. A., & Bailyn, C. D. 1997, ApJ, 477, 876
Orosz, J. A., Bailyn, C. D., McClintock, J. E., & Remillard, R. A. 1996, ApJ, 468, 380
Orosz, J. A., & Hauschildt, P. H. 2000, A&A, 364, 265
Orosz, J. A., Jain, R. K., Bailyn, C. D., McClintock, J. E., & Remillard, R. A. 1998, ApJ, 499, 375
Orosz, J. A., Kuulkers, E., van der Klis, M., et al. 2001, ApJ, 555, 489
Orosz, J. A., McClintock, J. E., Remillard, R. A., & Corbel, S. 2004, ApJ, 616, 376
Orosz, J. A., Polisensky, E. J., Bailyn, C. D., et al. 2002, BAAS, 34, 1124
Orosz, J. A., Steiner, J. F., McClintock, J. E., et al. 2011, ApJ, 730, 75
Özel, F., Psaltis, D., Narayan, R., & McClintock, J. E. 2010, ApJ, 725, 1918
Remillard, R. A., Orosz, J. A., McClintock, J. E., & Bailyn, C. D. 1996a, ApJ, 459, 226
Remillard, R. A., Orosz, J. A., McClintock, J. E., & Bailyn, C. D. 1996b, ApJ, 459, 226
Reynolds, M. T., Callanan, P. J., & Filippenko, A. V. 2007, MNRAS, 374, 657
Reynolds, M. T., Callanan, P. J., Robinson, E. L., & Froning, C. S. 2008, ApJ, 387, 788
Sanwal, D., Robinson, E. L., Zhang, E., et al. 1996, ApJ, 460, 437
Shahbaz, T., Naylor, T., & Charles, P. A. 1994, MNRAS, 268, 756
Shahbaz, T., van der Hooft, F., Casares, J., Charles, P. A., & van Paradijs, J. 1999, MNRAS, 306, 89
Shahbaz, T., van der Hooft, F., Charles, P. A., Casares, J., & van Paradijs, J. 1996, MNRAS, 282, L47
Shrader, C. R., Wagner, R. M., Hjellming, R. M., Han, X. H., & Starrfield, S. G. 1994, ApJ, 434, 698
Sunyaev, R. A., Kaniovsky, A. S., Borozdin, K. N., et al. 1993, A&A, 280, L1
Timmer, J., & Koenig, M. 1995, A&A, 300, 707
Valsecchi, F., Glebbeek, E., Farr, W. M., et al. 2010, Nature, 468, 77
van der Hooft, F., Groot, P. J., Shahbaz, T., et al. 1997, MNRAS, 286, L43
van der Hooft, F., Heemskerk, M. H. M., Alberts, F., & van Paradijs, J. 1998, A&A, 329, 538
Wagner, R. M., Foltz, C. B., Shahbaz, T., et al. 2001, ApJ, 556, 42
Wagner, R. M., Kreidl, T. J., Howell, S. B., & Starrfield, S. G. 1992, ApJ, 401, L97
Webb, N. A., Naylor, T., Ioannou, Z., Charles, P. A., & Shahbaz, T. 2000, MNRAS, 317, 528
Wong, T.-W., Valsecchi, F., Fragos, T., & Kalogera, V. 2012, ApJ, 747, 111
Zurita, C., Sánchez-Fernández, C., Casares, J., et al. 2002, MNRAS, 334, 999